Inorganic Chemistry

pubs.acs.org/IC
Article

Small Cysteine-Rich Motif, Big Function—Metal-Driven Dimerization of the CopY C-Terminal Fragment

Aleksandra Hecel,* Arian Kola, Alicia Dominguez-Martin, and Daniela Valensin

Cite This: *Inorg. Chem.* 2025, 64, 22615−22630
Read Online

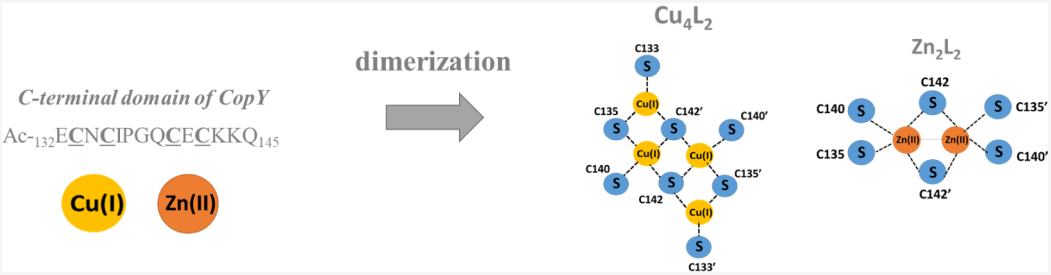

ABSTRACT: Transition metal homeostasis is essential for bacterial survival, especially under host-induced metal stress. The CopY repressor from *Enterococcus hirae* regulates copper levels through a conserved C-terminal CxCxxxxCxC motif, which binds metal ions such as Cu(I) and Zn(II) and modulates the DNA-binding activity of the protein. This work highlights the distinct coordination behaviors of Cu(I) and Zn(II) in the CopY C-terminal motif (Ac-ECNCIPGQCECKKQ) and sheds light on the structural basis of its metal-driven regulatory function. Using ESI-MS, potentiometry, UV−Vis, CD, NMR, and FT-IR, we show that this short sequence is sufficient for metal-driven dimerization and forms distinct complexes with Cu(I) and Zn(II). Cu(I) promotes the formation of binuclear (Cu_2L) and dimeric (Cu_4L_2) clusters, while Zn(II) favors monomeric (ZnL), bis-complex (ZnL_2), and minor dimeric (Zn_2L_2) forms. Metal binding induced significant structural rearrangements in the peptide, while the apo form was largely disordered; Zn(II) coordination stabilized more ordered conformations, and Cu(I) induced extensive conformational changes associated with the formation of distinct multinuclear complexes. These findings enhance our understanding of bacterial metallostasis and provide a molecular framework for future studies of metal-dependent gene regulation and antimicrobial strategies targeting metal homeostasis.

INTRODUCTION

Bacterial regulation of transition metal levels, also known as "metallostasis," refers to the mechanisms by which cells manage the internal availability of essential metal cofactors, avoiding both metal deprivation and toxicity. Metallostasis has emerged as a crucial aspect of the interaction between vertebrate hosts and pathogens, characterized by competition for nutrients. Hosts utilize various strategies to deprive pathogens of these essential metals or to control infections by the introduction of highly competitive metals. To counteract this, bacteria must adapt to these host-driven changes in metal availability by using specialized metal-sensing transcriptional regulators, called metalloregulatory proteins, and metallochaperones, which direct metals to their appropriate cellular locations.[1−4]

The CopY protein plays a crucial role in maintaining copper homeostasis, which is vital because copper serves as an essential cofactor for enzymes but becomes toxic when present in excess. The CopY repressor is found exclusively in Gram-positive bacteria and coordinates Cu(I) ions via a C-terminal CxCxxxxCxC motif. Interestingly, in *E. hirae*, when copper availability is low, CopY preferentially binds Zn(II),[5] forms a dimer, and activates the promoter of the copYZAB operon. CobineCobine *et al.* first demonstrated that this Zn(II)-bridged dimer is the physiological resting state of CopY.[6] In some species, CopY binds to Zn(II) in the absence of copper, maintaining its repressor function. When Cu(I) levels rise, copper displaces zinc, causing CopY to release from the DNA, which derepresses the target genes.[7] This Cu(I)-for-Zn(II) substitution is facilitated by direct Cu(I) transfer from the metallochaperone CopZ to CopY, as shown by Cobine et al.[8] Moreover, CopY also interacts with the chaperone CopZ, which is rather unique and has not been demonstrated for other Cu(I)-sensing transcriptional regulators.[9,10]

Understanding the function of CopY and the copper regulation system is essential, especially in bacteria, as copper

Received: July 14, 2025
Revised: October 2, 2025
Accepted: October 17, 2025
Published: November 7, 2025

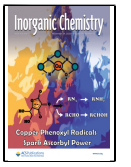

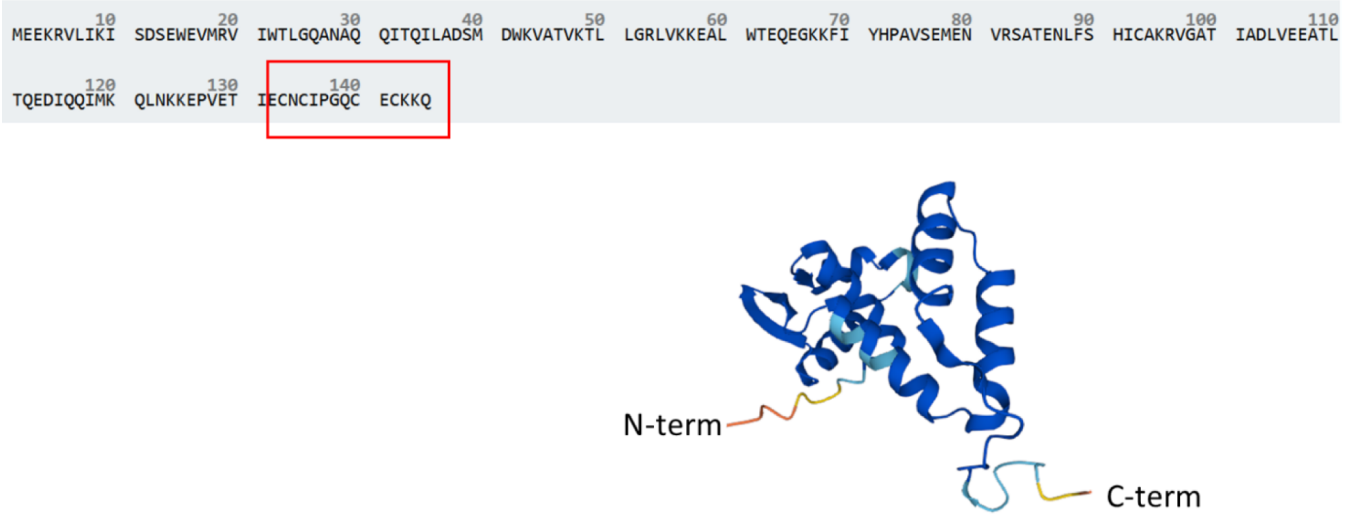

Figure 1. Amino acid sequence and 3D AlphaFold structure of the CopY protein (source: UniProt database Q47839); the analyzed sequence Ac-$_{132}$ECNCIPGQCECKKQ$_{145}$ is highlighted in red.

is widely used in antimicrobial strategies. Excessive copper can be toxic, and bacteria must precisely control its levels to survive. The study on CopY can offer insights into bacterial resistance mechanisms and help in developing treatments that exploit copper toxicity to kill pathogens. What is particularly important for this study is the fact that CopY, involved in copper homeostasis, can also bind Zn(II) ions.[10] Therefore, it is valuable to understand its coordination properties with Zn(II) and to compare their thermodynamic stability with that of copper complexes, to investigate whether Zn(II) could displace Cu(I) from its binding sites.

In this study, we focus on Cu(I) and Zn(II) complexes involving a C-terminal CxCxxxxCxC motif, which is involved in Cu(I) binding in *E.hirae* CopY: Ac-$_{132}$E**C**N**C**IPGQ**C**E**C**KKQ$_{145}$, highlighted in red in Figure 1. We elucidate their structural and thermodynamic properties using a variety of complementary methods: mass spectrometry provides information about complex stoichiometry, while potentiometry allows the determination of stability constants, enabling the identification of species present in the solution across different pH values. To analyze the ability of the CopY C-terminal CxCxxxxCxC motif to coordinate Cu(I) and Zn(II) in more detail, the peptide fragment was incubated with increasing amounts of metal ions, and the process was monitored using UV−VIS spectroscopy.

EXPERIMENTAL SECTION

Chemicals and Solutions. Ac-ECNCIPGQCECKKQ peptide (98% purity) was purchased from KareBay and used as received. The peptide was stored as a dry powder at −20 °C and handled exclusively inside a glovebox under an inert nitrogen atmosphere to prevent oxidation. Tetrakis(acetonitrile)copper(I) tetrafluoroborate [Cu(MeCN)$_4$BF$_4$] (Sigma-Aldrich) and 10% (v/v) acetonitrile were added to stabilize the Cu(I) oxidation state. Zn(II) perchlorate was an extra-pure product (Sigma-Aldrich). The concentrations of stock solutions of these salts were determined using inductively coupled plasma mass spectrometry. The carbonate-free stock solution of 0.1 M NaOH was purchased from Sigma-Aldrich and then potentiometrically standardized with potassium hydrogen phthalate.[11,12] All solutions were freshly prepared, thoroughly degassed to remove dissolved oxygen, and stored under an inert atmosphere. Peptide concentrations were determined using the DTNB (5,5′-dithiobis(2-nitrobenzoic acid)) assay directly inside the glovebox, ensuring the thiol groups remained in the reduced state. The peptide solutions were mixed with a freshly prepared 1 mM DTNB reagent in HEPES (pH 7.4) and incubated at room temperature for 15 min. The reaction resulted in the formation of the yellow 2-nitro-5-thiobenzoate anion (TNB^{2-}), which was quantified by measuring the absorbance at 412 nm using a UV−vis spectrophotometer. The concentration of free thiols was calculated using the molar extinction coefficient of TNB (ε = 14,150 M^{-1} cm^{-1}). All measurements were performed in duplicate inside a glovebox under an inert nitrogen atmosphere to prevent thiol oxidation. The DTNB-determined concentration consistently matched the peptide weight, confirming that the peptide was not oxidized. The concentration determined by DTNB consistently matched the theoretical peptide mass, indicating that the cysteine residues remained in their reduced thiol form. Therefore, the use of reducing agents such as DTT and TCEP was deemed unnecessary.

UV Titration of Ac-ECNCIPGQCECKKQ with Cu(I) and Zn(II). All titration experiments were performed using a 1 cm quartz cuvette, which was filled under strictly anaerobic conditions in a glovebox equipped with a palladium catalyst and filled with a 5% hydrogen/95% nitrogen gas mix. The apo-peptide was diluted in 20 mM Tris-HCl buffer, pH 7.4, with peptide concentrations of 20 μM. All UV spectra were recorded on a Jasco-730 spectrophotometer, situated in the glovebox, in the range of 190−800 nm. OriginPro 2016 was used to process and visualize the obtained spectra.

Mass Spectrometry. High-resolution mass spectra were obtained on a Bruker compact QTOF (Bruker Daltonik, Bremen, Germany), equipped with an electrospray ionization source with an ion funnel. The mass spectrometer was operated in positive ion mode. The instrumental parameters were as follows: scan range m/z 100−2000, dry gas—nitrogen, temperature 453 K, and ion energy 5 eV. The capillary voltage was optimized to achieve the highest S/N ratio, which was 4800 V. The samples were prepared in a 1:1 MeOH:H_2O mixture at pH 7 with an M:L molar ratio of 0.9:1, where $[ligand]_{tot}$ = 0.5 mM. The samples were infused at a flow rate of 3 μL min^{-1}. The instrument was calibrated externally with a Tunemix mixture (Bruker Daltonik, Germany) in quadratic regression mode. Data were processed by the application of the Compass DataAnalysis 4.2 (Bruker Daltonik, Germany) program. The mass accuracy for the calibration was better than 5 ppm, enabling, together with the true isotopic pattern (using SigmaFit), an unambiguous confirmation of the elemental composition of the obtained complex. Mass spectrometry experiments were carried out to qualitatively probe the Cu-peptide complex formation. At Cu:peptide ratios of 0.9:1 and 2:1 (data not shown), the spectra consistently showed dominant apo-peptide signals, with only weak peaks corresponding to Cu-bound species. This distribution does not reflect the actual solution

https://doi.org/10.1021/acs.inorgchem.5c03226
Inorg. Chem. 2025, 64, 22615−22630

equilibria, as potentiometric titrations under identical conditions indicate nearly complete metal binding. The discrepancy can be attributed to ionization and survival biases during electrospray, which are known to disfavor Cu−thiolate complexes. Even under conditions optimized for gentle ionization, apo-peptide signals typically remain more intense than those of metalated species.[13−15] We considered whether MALDI-MS might alleviate this problem, but previous reports and our own experience with similar Cu−peptide systems suggest that MALDI often promotes demetalation and matrix-induced artifacts, and therefore is unlikely to provide spectra dominated by intact complexes.[16,17] For this reason, we rely on potentiometry and complementary spectroscopies for quantitative speciation and present the MS data as qualitative support for the presence of Cu-bound forms rather than as a measure of their abundance.

Potentiometric Measurements. The stability constants for proton, Cu(I), and Zn(II) complexes with Ac-ECNCIPGQCECKKQ were calculated from titration curves carried out over the pH range of 2−11 at 298 K and an ionic strength of 0.1 M $NaClO_4$. The total volume of the solution used was 3.0 mL. The potentiometric titrations were performed using a Dosimat 800 Metrohm Titrator connected to a Metrohm 905 pH-meter and a Mettler Toledo pH inLab Science electrode. The thermostabilized glass cell was equipped with a magnetic stirring system, a microburet delivery tube, and an inlet−outlet tube for argon. Solutions were titrated with 0.1 M carbonate-free NaOH. The electrodes were calibrated daily for hydrogen ion concentration by titrating $HClO_4$ with NaOH using a total volume of 3.0 mL. The ligand concentration was 0.5 mM, and the metal-to-ligand ratio was 0.9:1. The exact concentrations and purities of the ligand solutions were determined by the Gran method. All samples were prepared inside a glovebox under an inert atmosphere and directly transferred to tightly sealed titration vessels. The vessels were wrapped with Parafilm and transferred to a potentiometric setup, where titrations were performed under a continuous argon stream to prevent oxidation. The following appropriate parameters were used: signal drift 1 mV min^{-1}; min waiting time 50 s, max waiting time 2000 s; volume increment 0.001 mL; and dosing rate 1 mL min^{-1}. The standard potential and the slope of the electrode couple were computed by means of the GLEE program.[18] The HYPERQUAD 2008 program was used for the stability constant calculations.[19] The speciation diagrams were computed with the HYSS program.[20] Overall stability constants (log β) obtained from potentiometric titrations were converted into overall dissociation constants (K_d) according to the following relationship: $K_d = 1/\beta$, where β is the cumulative formation constant for the given stoichiometry. It should be emphasized that these values are cumulative dissociation constants and not stepwise ones. They therefore describe the complete dissociation of each complex into free metal ion(s) and ligand and should not be interpreted as sequential steps of metal release.

NMR. Peptides were prepared in water containing 10% D_2O and 20 mM phosphate buffer at pH 7.4. The final peptide concentration was maintained at 0.5 mM. Zinc and copper ions were added from concentrated stock solutions of $Zn(NO_3)_2$ and $[Cu(CH_3CN)_4]BF_4$, respectively, to achieve the desired metal-to-peptide ratios. A 10 mM stock solution of $[Cu(CH_3CN)_4]BF_4$ was freshly prepared in 20 mM phosphate buffer (in D_2O, pH 7.4) containing 5% (v/v) acetonitrile. To minimize the oxidation of Cu(I) to Cu(II), ascorbic acid (1.0 mM final concentration) was added to peptide samples immediately prior to use. All solutions were degassed with water-saturated nitrogen and maintained under an inert N_2 atmosphere throughout the experiments.

NMR measurements were performed at 288 and 298 K using a Bruker Avance 600 MHz spectrometer. 3-(Trimethylsilyl)-[2,2,3,3-d_4]propane sulfonate, sodium salt, was used as the internal reference standard for NMR experiments. Spectral processing and analysis were conducted with TopSpin 3.6. To minimize the residual water signal, excitation sculpting was employed, applying a 2 ms selective square pulse centered on the water resonance.[21] Proton resonance assignments were obtained through two-dimensional NMR experiments, including the TOCSY and NOESY spectra.

FT-IR. FT-IR spectra were recorded by using an Agilent Cary 630 FTIR spectrometer equipped with a transmission module. Samples were prepared by depositing a small volume of a solution of the peptide and its Zn(II) complex in a phosphate buffer water solution. The solvent was allowed to evaporate completely under controlled ambient conditions. After evaporation, the resulting thin film or residue was analyzed directly.

RESULTS AND DISCUSSION

The Cu(I) and Zn(II) binding properties of the C-terminal CxCxxxxCxC motif of *E. hirae* CopY (Ac-ECNCIPGQ-CECKKQ) were investigated to elucidate their structural and thermodynamic characteristics. A combination of complementary techniques was employed: mass spectrometry provided information about complex stoichiometry, while potentiometric titrations facilitated the determination of stability constants and speciation across a wide pH range. UV−Vis spectroscopy was used to monitor spectral changes during incremental metal ion addition, offering insight into the coordination process. Structural details and conformational changes induced by metal binding were further explored through circular dichroism (CD), nuclear magnetic resonance (NMR), and Fourier-transform infrared (FT-IR) spectroscopy. The integration of these methods enabled a comprehensive description of both the metal coordination geometry and the accompanying structural rearrangements upon complex formation.

Stoichiometry of Cu(I) and Zn(II) Complexes with the C-Terminal Motif of CopY Protein. ESI-MS confirmed the stoichiometry of the Cu(I) and Zn(II) complexes with Ac-ECNCIPGQCECKKQ (Figure 2A and G). Table S1 shows the m/z values for both metal complexes at an M:L ratio of 0.9:1. ESI-MS peak assignments were based on the comparison between the precise calculated and experimental m/z values and their isotopic patterns.

On both MS spectra, the most intensive m/z signals correspond to the free ligand. The m/z values of 812.83 and 542.22 correspond to $[L]^{2+}$ (Figure 2B and H) and $[L]^{3+}$, respectively. The sodium ($[L + Na]^{2+}$, m/z = 823.81) and potassium ($[L + K]^{2+}$, m/z = 831.80) adducts of the free ligand were also detected. MS analysis confirmed the formation of dimeric forms the for Ac-ECNCIPGQCECKKQ ligand with m/z values of 1624.64 and 1084.10 for $[L_2]^{2+}$ and $[L_2]^{3+}$ (Figure 2D and J), respectively. Dimerization of the C-terminal motif of the CopY protein was confirmed before. Pazehoski etal. proved the specific involvement of the 38 C-terminal residues of CopY in dimerization.[22] From our studies, we can claim that an even shorter fragment (14 aa—ECNCIPGQ-CECKKQ) of the C-terminal *E. hirae* CopY fragment, containing the CxCxxxxCxC motif, is responsible for homodimerization.

In the case of metal complexes, for both copper and zinc complexes, the high-resolution mass spectra (Figure 2 and Table S1) reveal the formation of mononuclear species under the employed experimental conditions. The signals corresponding to the mononuclear Cu(I) and Zn(II) complexes are located at m/z values of 843.79 $[CuL]^{2+}$ (Figure 2C), 562.20 $[CuL]^{3+}$, 844.78 $[ZnL]^{2+}$ (Figure 2I), and 563.52 $[ZnL]^{3+}$, respectively. The polynuclear complexes were observed only for Cu(I) ions, where $[Cu_2L]^{2+}$ signal at m/z 875.81 was assigned (Figure 2E). In turn, bis-complexes were detected for zinc ions ($[ZnL_2]^{3+}$, m/z 1105.07 (Figure 2K)), which were not observed for copper.

https://doi.org/10.1021/acs.inorgchem.5c03226
Inorg. Chem. 2025, 64, 22615−22630

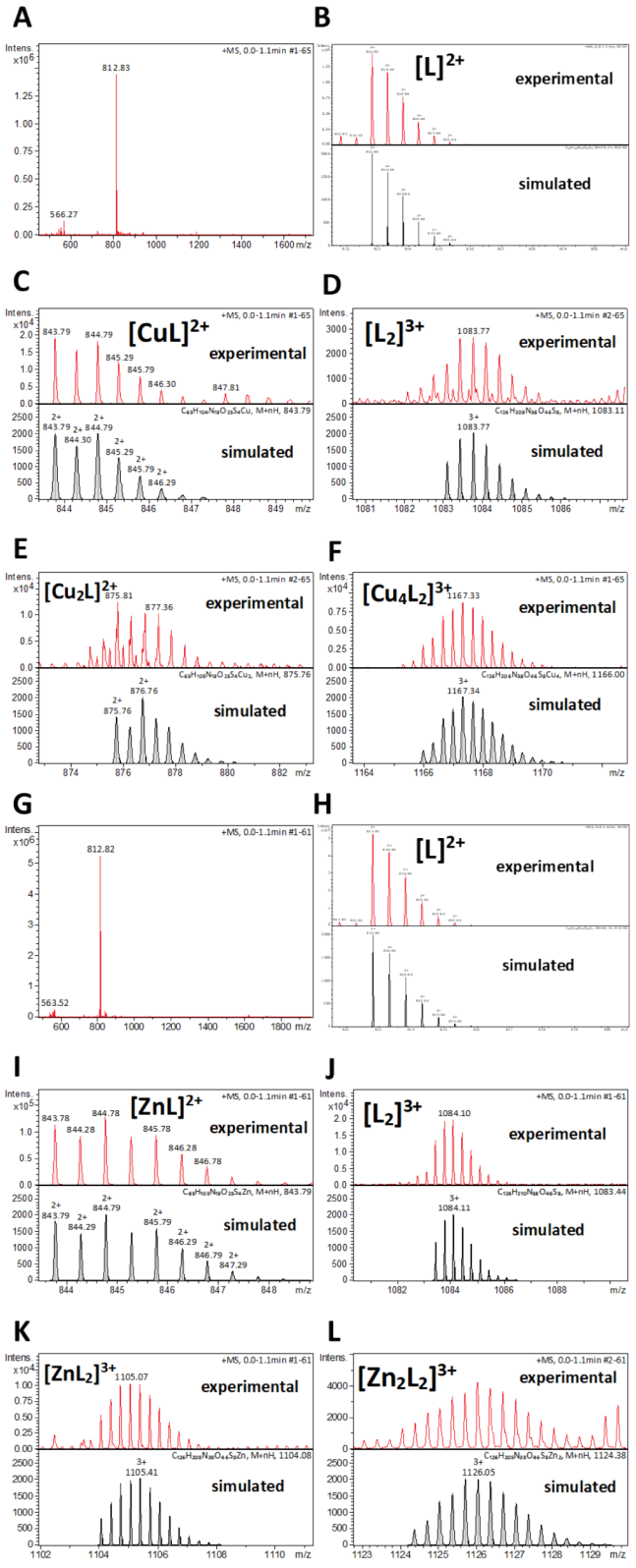

Figure 2. ESI-MS spectra of the A) Cu(II) and G) Zn(II)-Ac-ECNCIPGQCECKKQ systems. *M*:*L* molar ratio = 0.9:1. The complexes were prepared in a mixture of MeOH:H_2O (1:1) at pH 6. For the chosen ligand (B, D, H, J), Cu(I) (C, E, F), and Zn(II) (I, K, L) complexes, a comparison of experimental and simulated signals was performed.

The most unexpected *m*/*z* signals, with perfectly fitted isotopic patterns, were discovered for dimeric complexes. As suspected, apart from the dimer formation of the ligand itself, metal binding to the C-terminal region of CopY is also responsible for the homodimerization pathway in *Enterococcus hirae*. For copper, the signal corresponds to two ligands and four Cu(I) ions $[Cu_4L_2]^{3+}$ were detected at *m*/*z* 1167.33 (Figure 2F). For zinc, due to the fact that the monomeric form of the ligand binds up to one zinc ion, the dimer involves only two zinc ions, which were detected on MS spectra as $[Zn_2L_2]^{3+}$ signal with *m*/*z* at 1126.04 (Figure 2L).

Ligand Protonation and Formation of Metal Complexes in Solution. To analyze the metalation process in more detail and to obtain stepwise stability constants of Cu(I) and Zn(II) binding, potentiometric pH titrations are the method of choice. They are a specific and very precise tool to study metal−ligand interactions based on the change in pK_a values of the ligand groups in the absence and presence of metal ions. The C-terminal fragment of CopY features a total of nine protonation sites (Table 1). The three lowest proton dissociation constants (pK_a 2.48, 3.03, and 4.12, respectively)

Table 1. Equilibrium Constants and Proposed Coordination Modes for Cu(I) and Zn(II) Complexes with Ac-ECNCIPGQCECKKQ, *T* = 298 K, *I* = 0.1 M ($NaClO_4$), and *M*/*L* Molar Ratio = 0.9:1 (for Cu(I), Also *M*/*L* = 2:1).[a]

	log*β*	pK_a	Metal coordination
Ligand protonation			
H_9L	60.38(7)	2.48 (COOH)	
H_8L	57.90(7)	3.03 (E)	
H_7L	54.87(5)	4.12 (E)	
H_6L	50.75(7)	4.67 (C)	
H_5L	46.08(4)	7.90 (C)	
H_4L	38.18(3)	8.81 (C)	
H_3L	29.37(5)	9.13 (C)	
H_2L	20.24(3)	9.88 (K)	
HL	10.36(3)	10.36 (K)	
Cu(I) complexes (*M*:*L* molar ratio = 0.9:1)			
CuH_6L	56.18(3)		
CuH_5L	53.06(1)	3.12	$1S^-_{Cys}$
CuH_4L	49.37(3)	3.69	$2S^-_{Cys}$
CuH_3L	45.07(2)	4.30	$3S^-_{Cys}$
CuH_2L	39.75(3)	5.32	$4S^-_{Cys}$
CuHL	31.88(4)	7.87	$4S^-_{Cys}$, $H_2O/3S^-_{Cys}$, H_2O
Cu(I) complexes (*M*:*L* molar ratio = 2:1)			
Cu_2H_3L	49.31(2)		$3S^-_{Cys}$
Cu_2H_2L	45.61(1)	3.70	$4S^-_{Cys}$
Cu_2HL	40.77(2)	4.84	cluster formation Cu_2S_4
Cu_2L	33.32(3)	7.45	$4S^-_{Cys}$, $H_2O/3S^-_{Cys}$, H_2O
Zn(II) complexes (*M*:*L* molar ratio = 0.9:1)			
ZnH_7L	57.72(8)		
ZnH_6L	54.26(3)	3.46	
ZnH_5L	49.95(4)	4.31	$1S^-_{Cys}$
ZnH_3L	40.60(4)		
ZnH_2L	36.23(1)	4.37	$4S^-_{Cys}$
ZnHL	30.15(2)	6.08	$4S^-_{Cys}$, $H_2O/3S^-_{Cys}$, H_2O
ZnH_3L_2	64.51(4)		
ZnH_2L_2	58.36(5)	6.15	
$ZnHL_2$	48.27(5)	10.09	

[a]Values in parentheses are standard deviations on the last significant figure.

https://doi.org/10.1021/acs.inorgchem.5c03226
Inorg. Chem. 2025, 64, 22615−22630

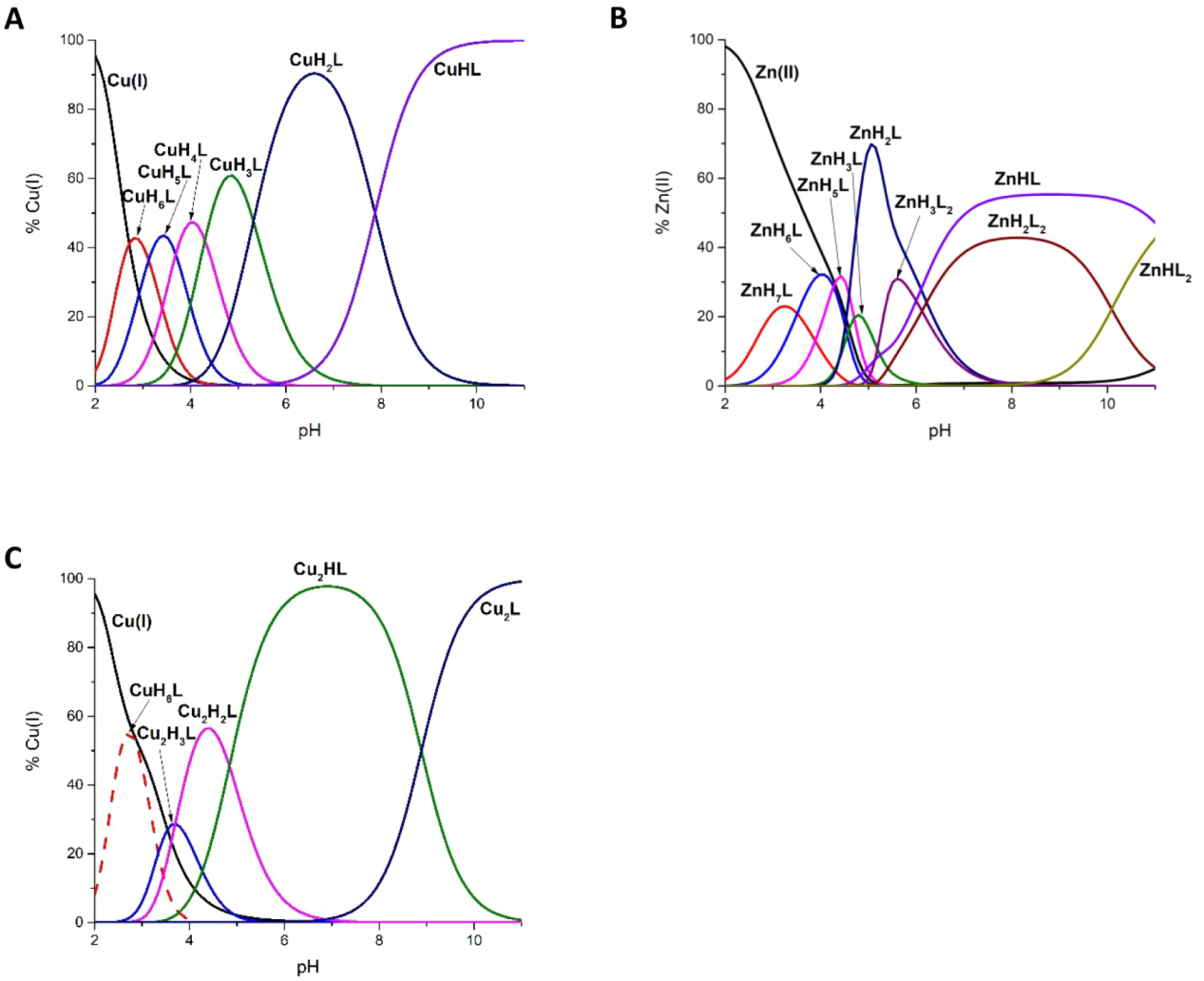

Figure 3. Species distribution diagrams of Cu(I) at (A) *M*:*L* = 0.9:1 and (B) *M*:*L* = 2:1, and Zn(II) (C) with Ac-ECNCIPGQCECKKQ, C_L = 0.0005 M.

correspond to the carboxylic acid groups of the C-terminal and the two glutamic acid side chains. These values are in good agreement with the literature, where the most acidic groups are detected in the pK_a range of 2−4.[23] For Ac-ECNCIPGQ-CECKKQ, the protonation constants of four cysteine residues were determined (pK_a 4.67, 7.90, 8.81, and 9.13). The dissociation constants of the Cys residues are usually found in the range between 8 and 9.[24−27] However, Freisinger et al. recently discovered a distinctive pK_a shift of (most likely) one cysteine thiolate group to a value of 4.3 when performing a potentiometric titration with the apo-metallothionein from the aquatic fungus *Heliscus lugdunensis*.[28] A possible explanation for one distinctively lower pK_a value of the Cys residue could be a strong hydrogen bond involving this Cys-thiolate group that would lower the pK_a value significantly. Possible H-bonding partners could be the two Lys residues or another still protonated Cys residue.[29,30] However, why this effect occurs only for one of the many thiolate groups present in the different MTs investigated remains unclear so far. Interestingly, for polyHis-tag proteins, which feature eight histidine residues, precisely one pK_a value assigned to His protonation is lower than usual. For example, for the DHDHDHHHHHHPGSSV-NH_2 (N-DpH) peptide, a pK_a of 4.70 was determined, while all other His residues have pK_a values in the range of 5.40−7.51.[31] The last two pK_a values of 9.88 and 10.36 come from the deprotonation of two lysine residues.

The complex formation constants and the calculated pK_a values of the C-terminal fragment of CopY in the presence of Cu(I) are shown in Table 1. To the best of our knowledge, this is the second case where potentiometry has been successfully applied to a Cu(I)-peptide system to obtain detailed insight into its binding properties.[32] The stability constants for Cu(I) complexes with Ac-ECNCIPGQCECKKQ were calculated on the basis of the titration curves recorded in the pH range of 2−11, as shown in Figure 3A. Potentiometric measurements revealed the presence of six equimolar complex species. Starting from a pH even below 2, the first detected species is CuH_6L, whose stoichiometry indicates that two glutamic acids and a carboxylic group of the C-terminus are deprotonated. Deprotonation and Cu(I) binding of the four following cysteine residues start from pH 2 and correspond to CuH_5L, CuH_4L, CuH_3L, CuH_2L species, respectively. The pK_a values for these Cu(I) complexes are within the range of 3.12−5.32 (Table 1). In the presence of Cu(I) ions, the pK_a values of the cysteine thiol groups decrease relative to the values of the apo form (4.67−9.13). Keeping in mind that copper(I), same as Zn(II), is normally unable to displace amide protons, the last calculated species, CuHL, with pK_a 7.87 corresponds to water

https://doi.org/10.1021/acs.inorgchem.5c03226
Inorg. Chem. 2025, 64, 22615−22630

molecule binding with $4S^{-}_{Cys}$, H_2O or $3S^{-}_{Cys}$, H_2O coordination mode. While coordination of the ε-amino group of a lysine side chain cannot be excluded in principle, several factors argue against this assignment in our system. The lysine ε-amino group has a relatively high intrinsic pK_a (∼10.5), making deprotonation at pH 7.5 unlikely; moreover, its hard donor character contrasts with the Cu(I) preference for softer ligands, and spectroscopic/potentiometric evidence from analogous systems consistently assigns pK_a values in the range of 7−8 to aqua ligands rather than lysine residues.[33−35]

Due to the fact that MS has confirmed the formation of dimeric Cu_2L species (Figure 2E), we decided to perform additional potentiometric titrations at a 2:1 *M*:*L* ratio. The first calculated species is Cu_2H_3L (Figure 3B and Table 1), where three of four cysteine residues are already deprotonated. This suggests that one Cu(I) ion can be coordinated by two cysteine residues, while the second Cu(I) is coordinated by only one at this stage. The next species, Cu_2H_2L, corresponds to two Cu(I) ions bound to all cysteine residues. The lowered pK_a value of 3.70, compared to the apo form (4.67), indicates the involvement of the last cysteine residue in complex formation (Table 1). An interesting phenomenon is observed for the Cu_2HL form with a pK_a of 4.84. This value is unlikely to be attributed to the deprotonation of an amide nitrogen, first because it is too low for an amide nitrogen, and second because Cu(I), with its completely filled d^{10} electron configuration, exhibits a behavior similar to that of Zn(II), where the displacement of the amide nitrogen by the coordinated metal is impossible,[36] or at least uncommon. The pK_a value of 4.84 is also too low to be assigned to the deprotonation of a water molecule. It should be emphasized, however, that the formal conversion from a terminal to a bridging thiolate does not itself require deprotonation; the observed pK_a should therefore be regarded as a macroscopic constant reflecting the net proton transfer associated with cluster reorganization.[37−39] Due to the lack of literature data on this topic, we can only speculate that this may result from the formation of a Cu_2S_4 cluster, where initially two copper ions were coordinated separately to two cysteinyl residues. At higher pH, structural rearrangement occurs, along with protonation/deprotonation of the cysteinyl residue (hence the pK_a value of 4.84) and the formation of a sulfide bridge between the two Cu(I) ions (Figure 4). The last Cu_2L species results from the deprotonation of a water molecule (pK_a = 7.45, Table 1).

The binding of Zn(II) to Ac-ECNCIPGQCECKKQ begins at a pH of about 2, and the first detected forms are ZnH_7L and ZnH_6L, where two (carboxylic groups of the C-terminus and glutamic acid) and three (carboxylic groups of the C-terminus and two glutamic acids) acidic residues are deprotonated, respectively (Table 1 and Figure 3C). The slightly lowered pK_a value of 3.46 for the Glu residue, compared to the apo form (pK_a = 4.12), may suggest its involvement in Zn(II) binding at very low pH. The next three species, ZnH_5L, ZnH_3L, and ZnH_2L, correspond to the binding of Zn(II) to cysteine residues. The $ZnH_3L \rightarrow ZnH_2L$ transition, indicated by pK_a = 4.31 (pK_a = 9.13 for the apo), corresponds to the binding of a fourth cysteine to Zn(II) and the generation of a [$4S^{-}$] coordination mode. For the ZnH_4L species, it was impossible to determine the stepwise dissociation constant due to the release of a proton within a very narrow pH range. The formation of the last ZnHL species (pK_a = 6.08) can be assigned to the deprotonation of a water molecule. Due to the

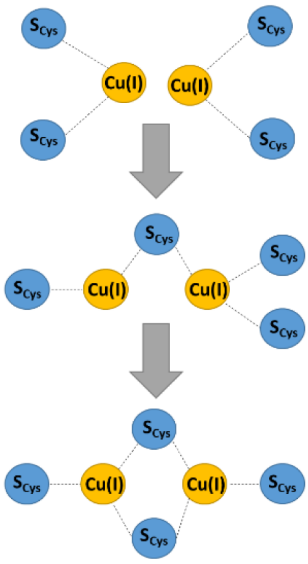

Figure 4. The proposed coordination mode of two Cu(I) ions to the C-terminal motif of the CopY protein Ac- ECNCIPGQCECKKQ. *M*:*L* ratio of 2:1, interpretation based on potentiometric studies.

fact that MS spectra (see Figure 2) confirmed the formation of both monomeric species and bis-complexes, stability constants for Zn(II) bis-complexes were also calculated. The bis-complexes start to appear at a pH of around 5−6 (Figure 3C). For the ZnH_2L_2 species (maximum concentration at pH 8), where all cysteine residues are deprotonated, the metal-binding mode could involve four His residues, two from each monomer. The amounts of monomeric (ZnHL ∼ 60%) and bis-complex (ZnH_2L_2 ∼ 40%) species are almost equal over a wide pH range between 7 and 9.

From potentiometric titrations, we were not able to calculate reliable log β values for dimeric or higher-order complexes (e.g., Zn_2L_2, Cu_4L_2). A likely explanation is that such species are indeed present in solution, even at a 1:1 *M*:*L* stoichiometry (as confirmed by MS), but their equilibrium concentrations are too low to be quantified potentiometrically. Moreover, Cu_2L (from potentiometry) and Cu_4L_2 (from MS), as well as ZnL and Zn_2L_2, all share an overall 2:1 M/L ratio; based solely on stoichiometry, potentiometry cannot easily discriminate between them because they contribute similarly to the overall proton balance (unless their protonation patterns differ significantly). To test this, we refitted the potentiometric data set in Hyperquad while explicitly including dinuclear and tetranuclear terms. During iterative refinement, both species were automatically excluded, as their calculated concentrations never exceeded ∼3−5% of total Cu, and their refined stability constants carried unrealistically high errors. This outcome reflects the limited sensitivity of potentiometry to species present in such low abundance, while MS can still detect them owing to its different bias toward ionization. Accordingly, our speciation model is based on mononuclear CuHL as the predominant solution species, with higher nuclearities present only in trace amounts, detectable by MS but below the threshold for reliable potentiometric refinement. Thus, the two techniques are complementary rather than contradictory: potentiometry robustly captures the predominant mononuclear species, while MS reveals the presence of higher-nuclearity complexes at lower abundance. Similar discrepancies between potentiometry and MS have been noted in related

https://doi.org/10.1021/acs.inorgchem.5c03226
Inorg. Chem. 2025, 64, 22615−22630

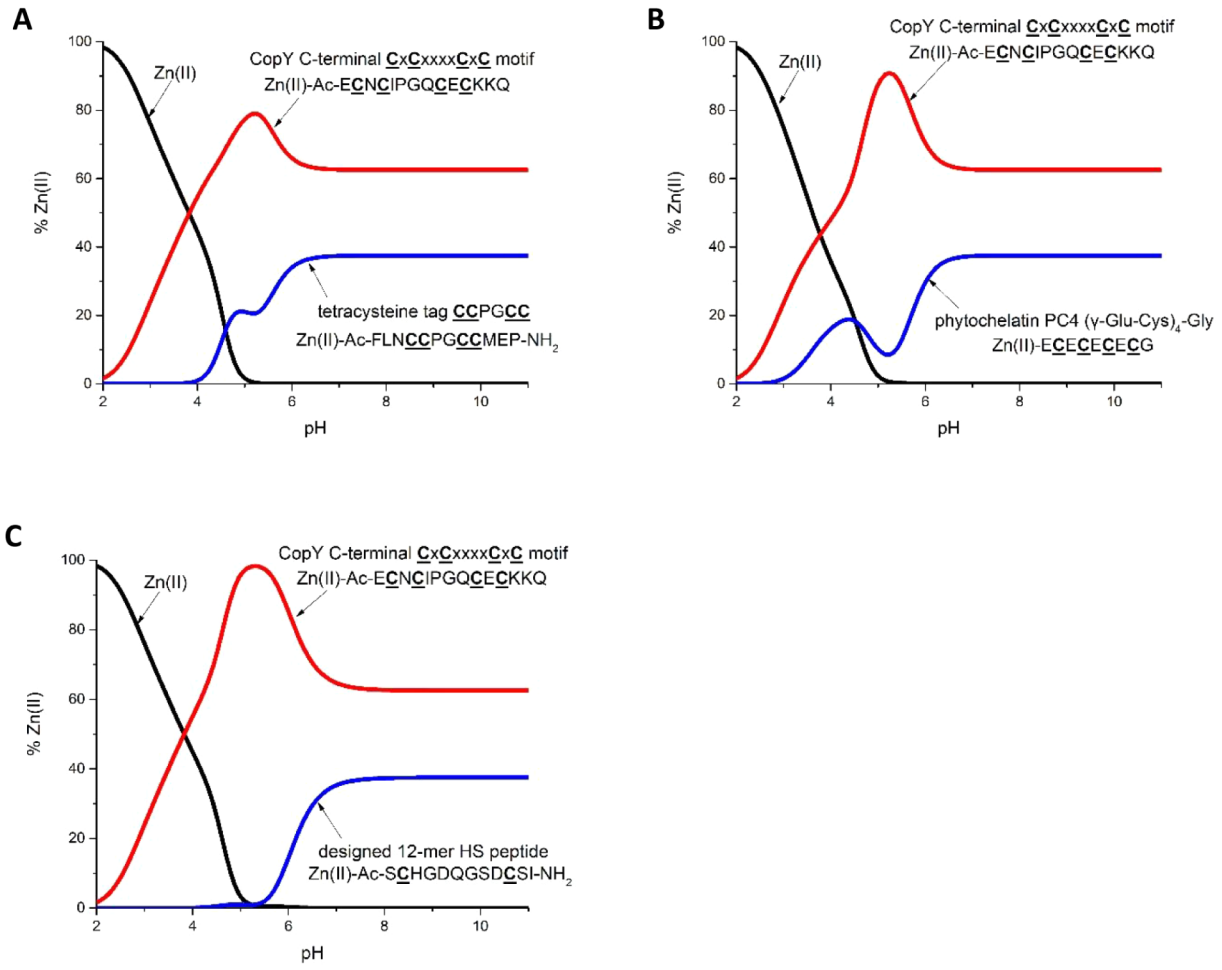

Figure 5. A competition plot between the C-terminal CxCxxxxCxC CopY motif (Ac-ECNCIPGQCECKKQ), Zn(II) ions, and A) a short tetracysteine tag Ac-FLNCCPGCCMEP-NH_2, B) phytochelatin PC4 (ECECECECG), and C) a designed 12-mer HS peptide (Ac-SCHGDQGSDCSI-NH_2). It describes complex formation at different pH values in a hypothetical situation in which equimolar amounts of all reagents are mixed. Calculations are based on binding constants from Table 1 and ref .[50−52].

peptide−metal systems, underscoring that minor multinuclear species, although detectable by MS, may fall below the threshold for reliable potentiometric refinement.[13,40] Moreover, complexes stabilized in solution primarily by weak or few intermolecular interactions generally exhibit low gas-phase stabilities and are prone to in-source dissociation during electrospray ionization.[41−44] Importantly, however, gas-phase stability does not necessarily parallel the solution binding affinity. For instance, even protein−ligand complexes stabilized by strong ionic interactions in solution may display unexpectedly low stability in the gas phase.[42]

The determination of overall stability constants is essential for understanding metal−protein interactions. Dissociation constant (K_d) values for Cu(I) and Zn(II) complexes were determined under physiologically relevant conditions (pH 7.4, ionic strength I = 0.1 M, 25 °C) by using potentiometric methods. The K_d calculated for the Zn(II) complex with the C-terminal CopY motif was found to be 1.64×10^{-14} M, indicating a high binding affinity within the picomolar range. This value aligns well with previously reported K_d values for Zn(II) binding to proteins or peptides coordinated by four cysteine residues. Specifically, metallothioneins (MTs) and shorter peptides, which utilize cysteine residues to tightly coordinate Zn(II), exhibit K_d values ranging from approximately 10^{-14} to 10^{-11} M.[45−47] These strong affinities highlight the biological significance of such proteins in zinc homeostasis and buffering. In the case of Cu(I), exceptionally low dissociation constants were determined for both 1:1 and 2:1 metal-to-ligand stoichiometries, with K_d values of 1.33×10^{-16} M and 2.19×10^{-19} M, respectively. These values correspond to pK_d values of approximately 15.9 and 18.7, indicating very tight binding in the subpicomolar to femtomolar range. Such high affinities are consistent with, or even exceed, those reported for known Cu(I)-binding proteins such as yeast Atx1, human Atox1, and engineered mutants like H48C-CopC, which typically exhibit K_d values in the range of 10^{-18} to 10^{-14} M.[48,49] Nevertheless, comparisons of absolute affinity values should be made with caution, as it has been demonstrated that different methodological approaches can yield divergent results for the same metal−ligand systems.[46]

Competitive Zn(II) Binding Highlights the Affinity of the CopY CxCxxxxCxC Motif. Since potentiometric data for Cu(I) complexes are not available, the comparison of the CxCxxxxCxC motif with other cysteinyl-containing sequences was limited to Zn(II) coordination. We focused on three systems: (i) a short tetracysteine tag, CCPGCC, which can be introduced at the *N*- or C-terminus of a protein or into flexible loops for *in vitro* or *in vivo* labeling with biarsenical probes;[50]

https://doi.org/10.1021/acs.inorgchem.5c03226
Inorg. Chem. 2025, 64, 22615−22630

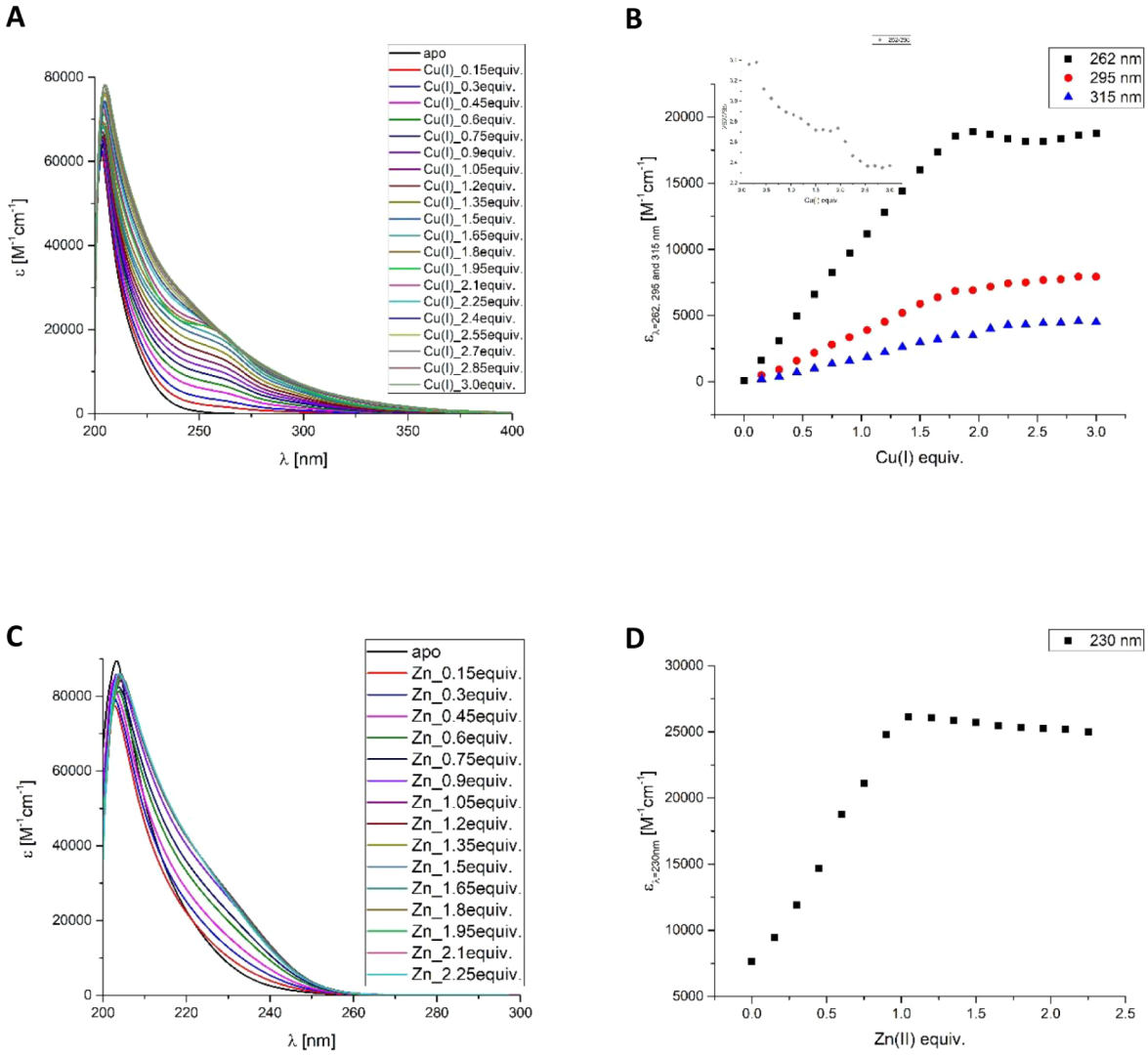

Figure 6. UV−vis titrations of Ac-ECNCIPGQCECKKQ with Cu(I) (A) and Zn(II) (C) in 20 mM Tris-HCl buffer, pH 7.4. Molar absorptivity values (ε) at 262, 295, and 315 nm (B) and at 230 nm (D) as a function of Cu(I) and Zn(II) equivalents, respectively. Additionally, the ratio of $\varepsilon_{(262)}/\varepsilon_{(295)}$ during the titration (B).

(ii) phytochelatin PC4, containing a repeating γ-Glu-Cys motif four times;[51] and (iii) a designed 12-mer HS peptide, Ac-SCHGDQGSDCSI-NH_2, whose sequence was inspired by the Cu(I)-binding loop of CueR from *Vibrio cholerae*.[52] To compare the thermodynamic stability of Zn(II) complexes with those of different ligands, competitive speciation diagrams were employed. These diagrams, based on the calculated stability constants, depict hypothetical scenarios in which equimolar amounts of ligands and Zn(II) ions are mixed. They enable a direct visual comparison of the relative affinities of the ligands toward the metal ion under similar conditions. Such comparative analysis is particularly valuable in the context of bioinorganic coordination chemistry, as it provides insight into how subtle differences in ligand architecture, such as cysteine spacing or backbone composition, can dramatically influence metal ion coordination, stability, and potentially biological function.

The CxCxxxxCxC motif derived from CopY displays a higher Zn(II) affinity than the canonical tetracysteine tag motif, CCxxCC (Figure 5A). This observation indicates that greater spatial separation of cysteinyl residues enhances the thermodynamic stability of Zn(II) complexes, compared to motifs where cysteine residues are positioned adjacently. The effect of the number of amino acid residues between two CxC units on Zn(II) complex stability was also examined (Figure 5B). The CopY CxCxxxxCxC motif again demonstrated superior binding properties relative to the PC4 CxCxCxC motif, in which only one amino acid separates the two CxC segments. In addition, a protein-derived fragment containing only two cysteine residues (Ac-SCHGDQGSDCSI-NH_2), despite forming Zn_2L bis-complexes in solution, the same as the C-terminal fragment of CopY, showed lower stability compared to the CopY motif, confirming the latter's enhanced metal-binding capacity.

Furthermore, when compared with cysteinyl motifs reported in the literature, the CopY CxCxxxxCxC sequence exhibits the strongest Zn(II) complexation based on potentiometric data, underscoring its exceptional thermodynamic stability and potential biological relevance.

Spectroscopic Evidence for Cu/Zn−Cys Cluster Formation. The metal ion binding ability and capacity were evaluated using spectrophotometric titrations of the apo-Ac-

https://doi.org/10.1021/acs.inorgchem.5c03226
Inorg. Chem. 2025, 64, 22615−22630

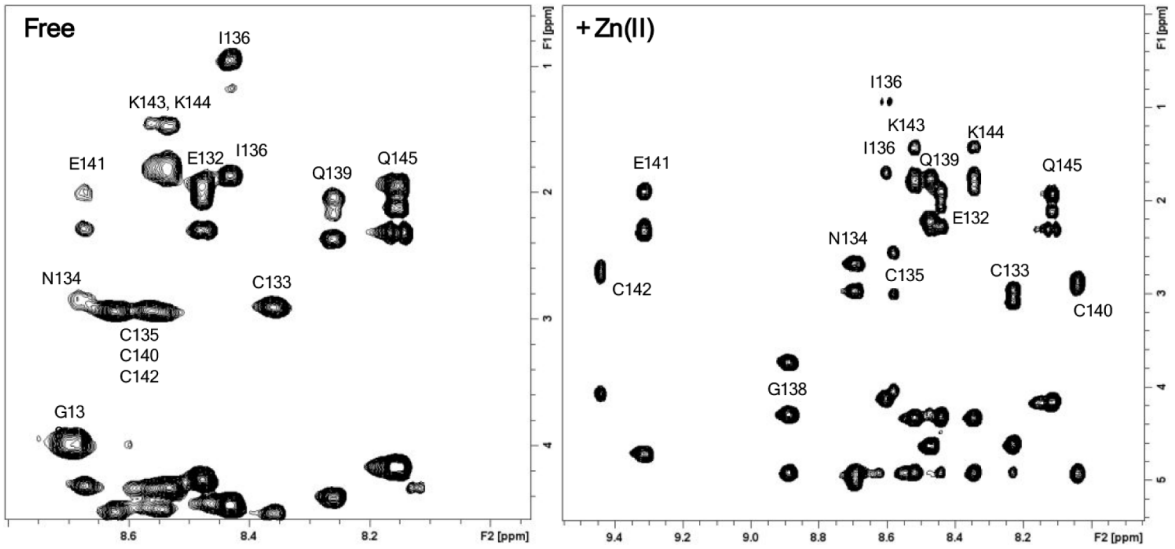

Figure 7. Fingerprint regions of $^{1}H-^{1}H$ TOCSY spectra of Ac-ECNCIPGQCECKKQ in the absence and presence of 0.9 Zn(II) equivalents. C_M = 0.5 mM, T = 288 K, 20 mM phosphate buffer, pH 7.4.

ECNCIPGQCECKKQ peptide with increasing amounts of Cu(I) and Zn(II) ions (Figure 6A and C, respectively). The addition of Cu(I) ions leads to the formation of a broad absorption envelope in the 250−400 nm range, and a shoulder at 262 nm has been assigned to the sulfur → copper(I) charge transfer band.[53,54] The intensity of the LMCT band at 262 nm increases roughly linearly up to 2.0 equiv of Cu(I), reaching ε_{max} values of roughly 20000 M^{-1} cm^{-1}, suggesting the binding of two Cu(I) ions strongly per monomer (Figure 6B). The next two bands in the UV−vis spectra at 295 and 315 nm are less clear, and the intensity of these bands increases linearly up to 1.8−2 equiv (Figure 6B). Consistent with thiolate-bridged cluster growth, the $\varepsilon_{262}/\varepsilon_{295}$ ratio decreases to ∼1.5, remains nearly constant up to ∼2.0 equiv of Cu(I), and then decreases further at higher loadings. This behavior may reflect an initial coordination of terminal cysteines to Cu(I), followed by the involvement of bridging thiolate bonds that stabilize higher-order Cu(I)−thiolate clusters. The UV region around 295 nm is indicative of Cu(I)-thiolate cluster formation, hence the formation of bridging thiolate groups, which seems to occur either for a binuclear Cu(I)-thiolate core (Cu_2L) or for a dimeric form, where two (Cu_2L_2) or four (Cu_4L_2) copper(I) ions are coordinated to a homodimer. Evidence of binuclear Cu(I)-thiolate core formation (Cu_2L) in the *E. hirae* CopY monomeric C-terminal motif has been presented in several papers,[7,9] while Cu_2L_2 species formation is not as obvious for this bacterial protein. A previous structural study of CopY from *Streptococcus pneumoniae* (*Spn*) revealed that the C-terminal fragment of *Spn* CopY exists as a homodimer in solution and binds up to two Cu(I) ions.[55] One difference, which may have a huge influence on dimer formation in the presence of Cu(I) ions for the C-terminal fragment of CopY from *Spn,* is the fact that *Spn* sequence alignment of the CopY protein reveals only one CxC motif at the C-terminus, while CopY from *Enterococcus hirae* has four cysteine residues, forming a CxCxxxxCxC motif. The cluster formation between Cu(I) and cysteine residues was confirmed by copper(I) titration (Figure 6A) and showed that up to two Cu(I) ions could be bound by one monomer, while ligand dimerization could provide Cu_4L_2 cluster mode,[5] which was also confirmed by MS spectra (Figure 2 and Table 1S). The Cu_2L_2 species was not observed in the MS spectra; thus, we can conclude that one CxC motif presented e.g., in CopY from *Streptococcus pneumoniae* or *S. mitis* forces the C-terminal fragment to create a Cu_2L_2 complex, while two CxC motifs in the C-terminal fragment of CopY (e.g., *Enterococcus hirae* and *Lactobacillus*) cause Cu_4L_2 homodimer formation.

Development of the ligand-to-metal charge transfer (LMCT) band associated with metal−thiolate bond formation was monitored at 230 nm for Zn(II) binding, as previously described (Figure 6C).[28,56] The intensity of the LMCT band (Cys → Zn(II)) increases progressively and reaches a plateau after the addition of 1.0 equiv of metal ions (Figure 6D), consistent with the formation of a stoichiometric Zn-thiolate complex. This behavior is in excellent agreement with speciation models derived from potentiometric titrations, which revealed the predominant presence of mononuclear ZnL and bis-complex ZnL_2 species. Mass spectrometry likewise did not provide evidence of the presence of polynuclear complexes per monomer. Together, these results confirm that Zn(II) favors the formation of simple, well-defined complexes that stabilize the local structure, in contrast to the multinuclear cluster formation observed for Cu(I).

Structural Properties of CopY and Its Cu(I) and Zn(II) Complexes. NMR measurements were conducted by solubilizing the peptide in 20 mM phosphate buffer at pH 7.4. Initially, the NMR spectra were recorded at 298 K; however, the visibility of the NH signals was limited. Therefore, the temperature was lowered to 288 K in order to slow down proton exchange and enhance the intensity of the amide proton signals. 1D and 2D $^{1}H-^{1}H$ TOCSY and NOESY spectra were recorded both in the absence and presence of 0.9 equiv of metal ions (Zn(II) and Cu(I)) in order to identify the residues involved in the metal coordination sphere and to assess any conformational changes upon Zn(II) and Cu(I) binding. The free ligand exhibited 1D and 2D NMR spectra, characteristic of a highly flexible and intrinsically disordered peptide. In particular, the 2D NOESY spectra displayed no inter-residue NOE correlations, indicating the absence of stable long-range contacts (Figure S1). By contrast, in the presence of metal ions, the NOESY spectra revealed nontrivial NOE correlations (Figure S1), supporting

https://doi.org/10.1021/acs.inorgchem.5c03226
Inorg. Chem. 2025, 64, 22615−22630

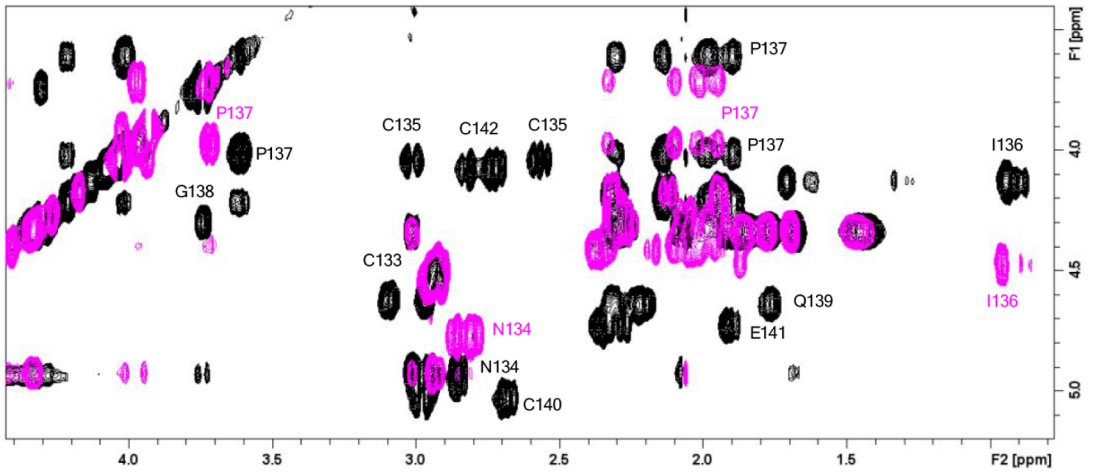

Figure 8. The aliphatic regions of $^{1}H-^{1}H$ TOCSY spectra of Ac-ECNCIPGQCECKKQ in the absence (magenta) and in the presence of 0.9 Zn(II) equivalents (black). C_M = 0.5 mM, T = 288 K, 20 mM phosphate buffer, pH 7.4.

the metal-induced rearrangement of the peptide backbone (*see infra*).

The NMR spectrum following Zn(II) addition revealed several key effects (Figure S2). First, an increased dispersion of amide proton signals was observed in the fingerprint region of the TOCSY spectrum, suggesting a shift toward a more structured conformation upon Zn(II) coordination (Figure 7). In addition to the overall chemical shift changes, zinc coordination leaves the NMR line widths of the peptide signals unchanged and wellresolved, thereby indicating the formation of monomeric Zn(II) complexes (Figure S3). Consistently, marked chemical shift variations were observed for specific amino acids, notably cysteine and adjacent residues (Figures 8 and 9). As graphically shown in the histograms of Figure 9, the metal ion induces chemical shift variations in both backbone and side-chain protons, indicating that Zn(II) binding not only influences the cysteines but also impacts nearby residues, potentially altering the local structure. By analyzing the Hβ protons of the cysteine residues in the presence of Zn(II), Cys135 stands out among the four, displaying a clear diastereotopic splitting of the Hβ signals, with one of the two protons shifted upfield by approximately 0.40 ppm. Cys133 also exhibits a diastereotopic shift, with one of the Hβ protons shifted downfield by about 0.20 ppm. Cys142 shows a comparable variation, with an upfield shift of 0.20 ppm. Finally, the Hβ protons of Cys140 appear to be the least affected, showing a modest upfield shift of 0.06 ppm. A completely different trend is observed when examining the backbone protons (HN and Hα). In this case, Cys140 and Cys142 exhibit the most pronounced effects on the amide protons, which are shifted upfield by 0.5 ppm for Cys140 and downfield by 0.9 ppm for Cys142. Regarding the Hα protons, Cys135, Cys140, and Cys142 show shifts of comparable magnitude; however, Cys135 and Cys142 experience upfield shifts, whereas Cys140 is shifted downfield. In contrast, Cys133 shows only a minimal change in its Hα proton, with a downfield shift of less than 0.07 ppm. All these effects, in addition to confirming the interaction of Zn(II) with the four cysteine residues, indicate that the peptide undergoes substantial structural rearrangements upon metal coordination. This is further supported by the observation of significant chemical shift variations for the backbone NH of several other residues located between positions 136 and 141, suggesting that the binding of Zn(II) induces conformational changes that extend beyond the immediate coordination sphere. In particular, Zn(II) coordination by the four cysteine residues promotes a peptide refolding that brings Cys135 and Cys140 into close proximity. This conformational rearrangement is essential to enable tetrahedral coordination geometry. Conversely, the inherent spatial proximity between Cys133/Cys140 and Cys135/Cys142 results in a reduced structural impact on the terminal regions of the peptide, as reflected by the more limited chemical shift perturbations observed in those areas.

This pattern of shifts suggests a structural influence on this intervening region, potentially organizing it into a specific secondary structure upon Zn(II) binding. The observed chemical shift variations, particularly in the backbone amide and Hα protons between residues 136 and 141, support the hypothesis that metal coordination may drive the formation of defined local conformations. To explore this possibility, Chemical Shift Index (CSI) analysis was performed to assess the presence and type of secondary structure elements induced by Zn(II) coordination. CSI is a technique used to predict protein secondary structures by examining variations in the chemical shifts of Cα or Hα atoms. This method involves comparing the measured chemical shift values of each amino acid to the expected values for a random coil conformation, allowing for the identification of deviations that may suggest α-helices, β-sheets, or disordered structures. Positive CSI values (upfield deviations) typically indicate α-helices, while negative values (downfield deviations) are associated with β-sheets. Values near zero or without a clear trend are generally indicative of random coils or disordered regions. Figure 10 reports the graph of the CSI of the Zn(II)-Ac-ECNCIPGQ-CECKKQ complex, obtained by assigning a value of −1 to the upfield $^{1}H\alpha$ chemical shift variations of residues exceeding 0.10 ppm, +1 to the residues with chemical shift variations greater than 0.1 ppm, and 0 for residues where the chemical shift does not deviate upfield or downfield by more than 0.1 ppm.

The CSI data suggest that Zn(II) coordination promotes the formation of defined secondary structure elements in the central region of the peptide, with a β-strand-like pattern extending from N134 to E141. Moreover, the pronounced CSI deviations observed for Cys135 and Cys142 may also reflect electronic effects associated with direct metal coordination

https://doi.org/10.1021/acs.inorgchem.5c03226
Inorg. Chem. 2025, 64, 22615−22630

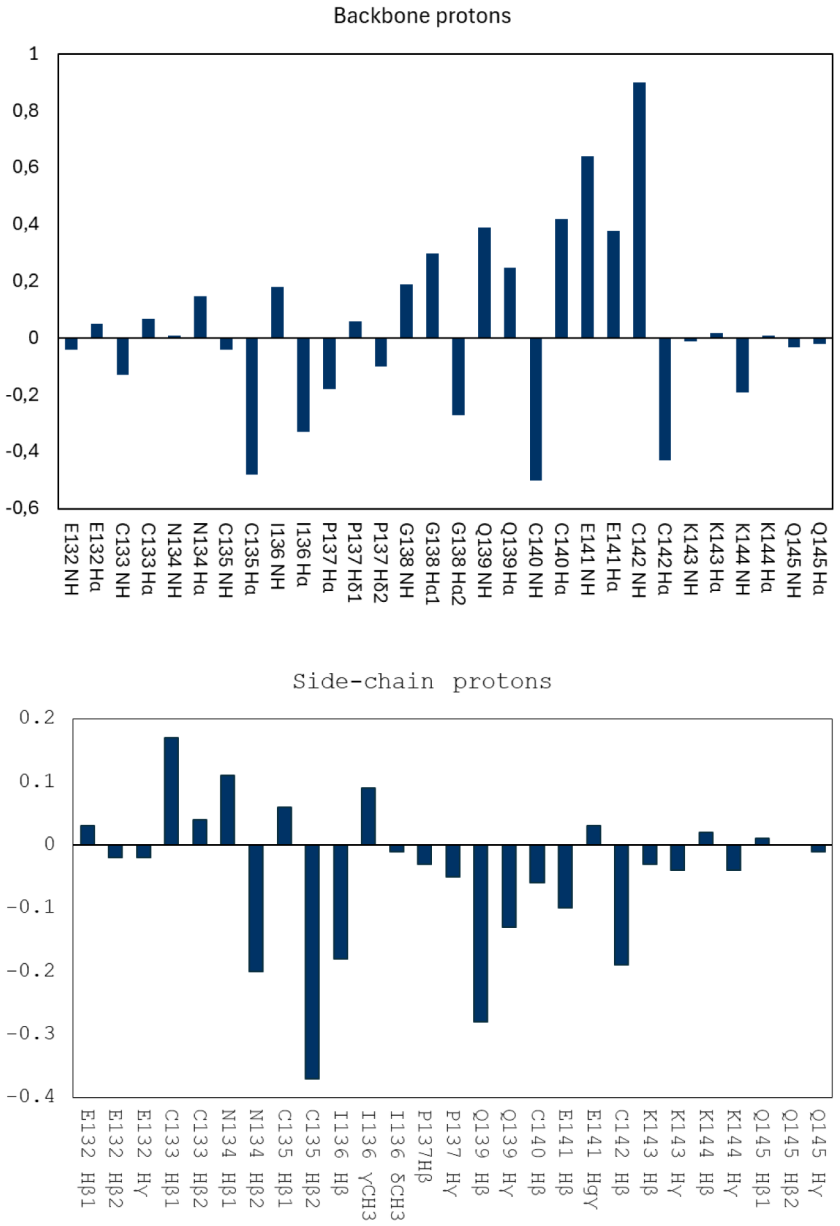

Figure 9. Chemical shift variations ($\Delta\delta$, ppm) observed upon the addition of 0.9 equiv of Zn(II) to Ac-ECNCIPGQCECKKQ. The upper panel shows the changes in backbone proton resonances (HN and Hα), while the lower panel displays the variations for side chain protons. C_M = 0.5 mM, T = 288 K, 20 mM phosphate buffer, pH 7.4.

rather than local secondary structure alone. In addition to these observations, the NOESY spectrum provided further insights. The NOE correlations in the presence of Zn(II) were considerably more pronounced than those in the free peptide spectrum (Figures S1 and S4). Furthermore, characteristic intermolecular correlations were observed, indicative of secondary structure elements. Notably, strong NH-Hα correlations suggested the formation of a β-strand or another organized secondary structure.

To further investigate this aspect, CD and FT-IR spectra of the peptide were recorded in the absence and presence of Zn(II) (Figure 11). The CD spectra of the peptide provide clear evidence for Zn(II)-induced conformational changes. In the absence of Zn(II), the peptide exhibits a strong negative band centered around 200 nm, which is characteristic of a largely disordered or random coil structure. However, the presence of a small negative band in the 220−230 nm range could indicate a slight tendency of the peptide to adopt an α-helical structure. Upon the gradual addition of Zn(II) (0.5 to 2.0 equiv), the spectral profile undergoes significant alterations: the intensity of the 200 nm minimum decreases, while a positive band at around 215−220 nm becomes certainly pronounced (Figure 11A). These changes are consistent with the formation of ordered secondary structure elements, likely β-strands or turn-like conformations, promoted by metal coordination. The progressive nature of the spectral shift suggests a metal-induced folding event, in agreement with CSI analysis and the hypothesis that Zn(II) binding stabilizes a more compact and structured peptide conformation. The FT-IR spectra further confirm Zn(II)-induced conformational changes in the peptide (Figure 11B). In the apo form, the strong amide I band around 1655 cm^{-1} is indicative of a predominantly disordered structure. Upon metal binding, the intensity of both the amide I and amide II bands decreases, and

https://doi.org/10.1021/acs.inorgchem.5c03226
Inorg. Chem. 2025, 64, 22615−22630

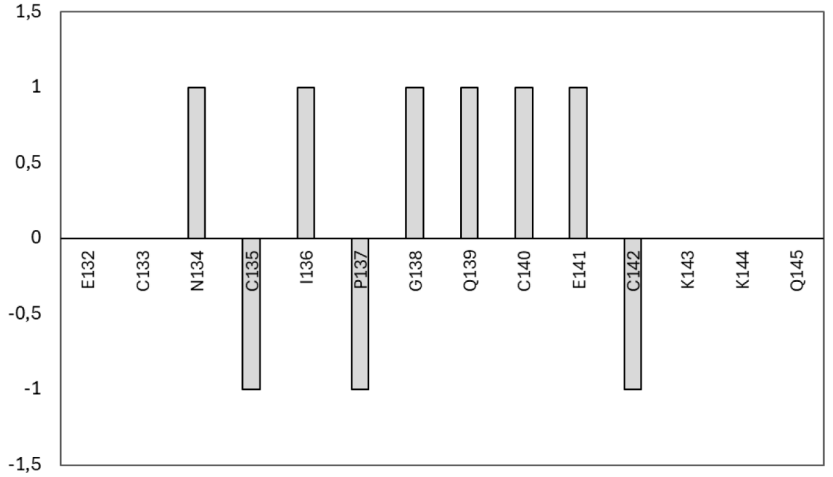

Figure 10. The chemical shift index of Hα protons of the Zn(II)-Ac-ECNCIPGQCECKKQ complex.

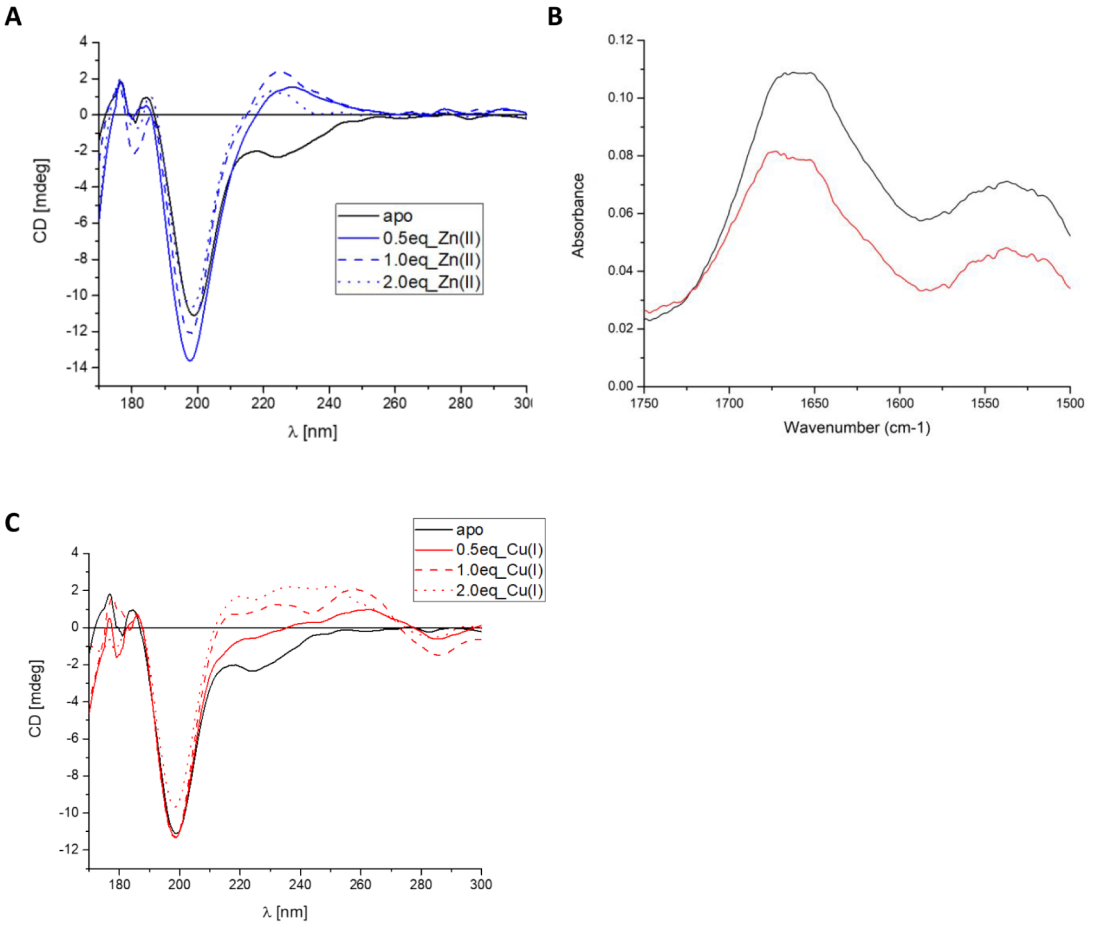

Figure 11. A) Far-UV CD spectra of the Ac-ECNCIPGQCECKKQ peptide, recorded in the absence (apo) and presence of 0.5, 1.0, and 2.0 equiv of Zn(II). (B) FT-IR spectra of the Ac-ECNCIPGQCECKKQ peptide in the dry state, recorded in the absence (black line) and presence of Zn(II) at 1.0 equiv (red line). C) Far-UV CD spectra of the Ac-ECNCIPGQCECKKQ peptide, recorded in the absence (apo) and presence of 0.5, 1.0, and 2.0 equiv of Cu(I). C_L = 0.5 mM, T = 298 K, 20 mM phosphate buffer, pH 7.4.

a slight shift toward lower wavenumbers is observed. These spectral changes are consistent with the formation of more ordered secondary structure elements and support the structural rearrangement suggested by the CD and CSI data.

A similar analysis was also conducted for the peptide complex with the cuprous ion. Similar to the zinc case, the addition of copper led to a greater dispersion of the NH signals in the NMR spectrum (Figure S5). However, unlike the previous observations, the spectrum shows multiple analogous spin systems and line broadening (Figure S3), suggesting the presence of several species coordinated to Cu(I) in solution. At the same time, the comparison of the spectra recorded for Zn(II) and Cu(I) complexes excluded the formation of identical metal complexes, as shown by the fact that no

https://doi.org/10.1021/acs.inorgchem.5c03226
Inorg. Chem. 2025, 64, 22615−22630

NMR signal was superimposed on the ones corresponding to the Zn(II) complex (Figures S1 and S3). Unfortunately, the presence of multiple species in solution prevented the complete assignment of the NMR spectrum, thereby also hindering the acquisition of information on the coordination sphere and the conformational rearrangements induced by Cu(I).

A fascinating phenomenon is observed in the CD spectra (Figure 11C) when the apo peptide is titrated with 0.5, 1.0, and 2.0 equiv of Cu(I) ions. The addition of 0.5 equiv of Cu(I) ions causes the disappearance of the negative absorption band at 220−230 nm, characteristic of the apo peptide, and the emergence of a positive band at 260 nm. With one equivalent of Cu(I) ions, two positive bands are observed: a more intense band at 260 nm compared to 0.5 equiv of Cu(I) and a broad positive band in the range of 210−240 nm. At a 1:1 metal-to-ligand (*M*:*L*) ratio, a dinuclear Cu_2L and dimeric Cu_4L_2 complex are detected, as previously confirmed by UV−vis and MS studies. Here, we can have a mixture of monomeric CuL, dinuclear Cu_2L, and dimeric Cu_4L_2 complex forms. The enhanced formation of dinuclear and dimeric species becomes evident upon the addition of 2.0 equiv of copper ions, as indicated by a very broad positive band in the CD spectrum between 220 and 260 nm, which may suggest a predominance of the Cu_2L and Cu_4L_2 complex forms.

The CD spectra of Zn(II) complexes also differ from that of the apo peptide, but their shapes remain very similar regardless of the Zn:L ratio (Figure 11B). Spectroscopic and MS studies have revealed that the C-terminal motif of the CopY protein can bind up to one Zn(II) ion, forming either monomeric ZnL or dimeric Zn_2L_2 complexes. As observed in the CD spectrum, these complexes show no structural differences (1.0 and 2.0 equiv of Zn(II)). The bis-complexes ZnL_2, particularly in the presence of 0.5 equiv of Zn(II), could also form (as confirmed for a 1:1 ratio by MS and potentiometry). However, as observed, their conformations do not differ significantly from those of the ZnL and ZnL_2 complexes.

Proposed Coordination Models of Cu(I) and Zn(II) Complexes. To provide a clearer understanding of the coordination pathways of Cu(I) and Zn(II) with cysteine residues in the C-terminal motif of the CopY protein, Figure 12 presents schematic models of the main complex species. Based on the combined spectroscopic (UV−vis, CD, NMR, FT-IR), potentiometric, and mass spectrometric data, we propose a set of coordination modes that rationalize the observed metal−peptide interactions.

For Cu(I), the data support the sequential formation of mononuclear (CuL), binuclear (Cu_2L), and higher-order dimeric (Cu_4L_2) species. The conserved CxCxxxxCxC motif provides a suitable arrangement of thiolate donors to support bridging coordination, enabling cluster formation even within a relatively short peptide sequence. The predominance of Cu_2L and Cu_4L_2 species observed in MS and supported by characteristic UV−vis features, such as the broad absorption and $S^- \rightarrow Cu(I)$ charge transfer band at 262 nm, strongly suggests a thiolate-driven multidentate coordination mode.

In contrast, Zn(II) forms primarily monomeric (ZnL), biscomplex (ZnL_2), and dimeric (Zn_2L_2) species, with no evidence of higher-nuclearity clusters. The Zn(II)-induced conformational changes observed in CD and NMR spectra imply a more structured peptide conformation upon metal binding, but without the extensive thiolate bridging seen in Cu(I) complexes. This difference highlights the distinct

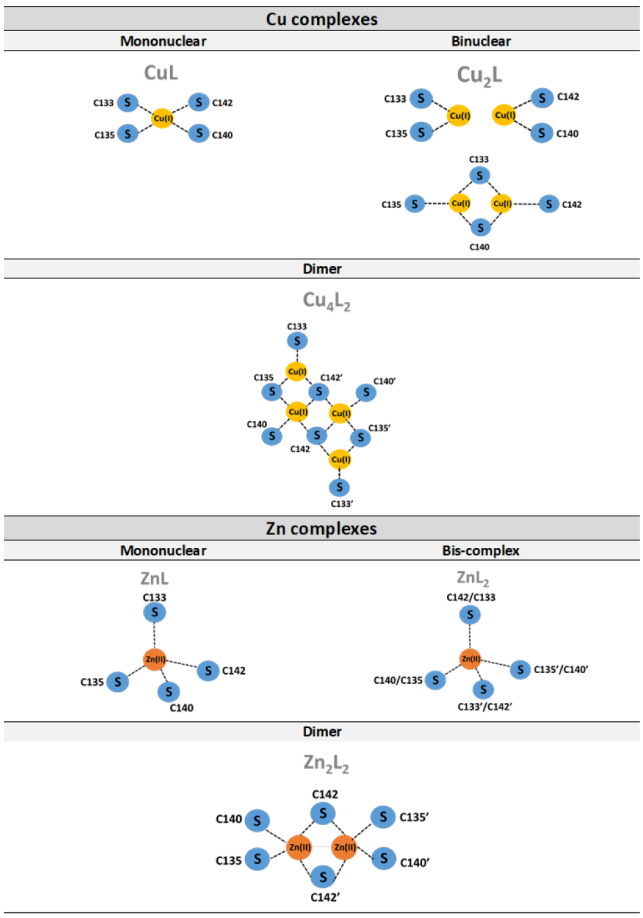

Figure 12. Proposed coordination modes and stoichiometries of Cu(I) and Zn(II) complexes with the C-terminal motif of CopY, based on the ESI-MS data. Cu(I) forms predominantly binuclear (Cu_2L) and dimeric cluster-type (Cu_4L_2) species, in addition to mononuclear (CuL) complexes. Zn(II), in contrast, favors the formation of monomeric (ZnL), biscomplex (ZnL_2), and dimeric (Zn_2L_2) species without evidence of higher-order cluster formation. Cysteine residues involved in metal coordination are labeled, and potential bridging interactions are indicated. Coordinating water molecules at elevated pH, as suggested by potentiometric data, are omitted for clarity.

coordination chemistry of Cu(I) and Zn(II) and their differing preferences for cluster formation versus discrete complex species.

Together, these proposed models emphasize how the spatial arrangement of cysteine residues governs not only the stoichiometry but also the structural organization of metal-peptide assemblies, potentially linking metal coordination to functional dimerization and regulatory activity of CopY. It is worth noting that Cobine et al. have extensively characterized the coordination environment of Cu(I) and Zn(II) ions in the full-length CopY protein using spectroscopic, luminescence,[6] and XAS techniques,[8] providing a foundational model for Cu/Zn−S binding in this system. Importantly, the C-terminal CopY motif investigated here contributes directly to the metal coordination observed in the intact protein. This conclusion is consistent with the work of Pazehoski et al.,[22] who demonstrated that the 38-residue C-terminal fragment of CopY from *Enterococcus hirae* exhibits the same coordination pattern, further supporting the central role of this domain in metal binding and dimerization. Taken together, these studies

https://doi.org/10.1021/acs.inorgchem.5c03226
Inorg. Chem. 2025, 64, 22615−22630

show that whether considering the full-length protein, the 38-residue C-terminal construct, or the shorter 14-residue motif analyzed here, the Cu(I)/Zn(II) coordination mode remains conserved. This validates the use of truncated C-terminal fragments as reliable and simplified models for probing the metal-binding properties of CopY. Our study builds upon this established framework by integrating potentiometric and mass spectrometry methods, which allow us to refine and deepen the understanding of cluster interactions with the C-terminal fragment of CopY. Thus, while the coordination mode we observe closely resembles that reported by Cobine et al., our multidisciplinary approach provides novel insights into the thermodynamic and structural aspects of metal binding.

CONCLUSIONS

This study provides new insights into the metal-binding properties of the C-terminal fragment of the CopY protein from *Enterococcus hirae*. We demonstrated that a 14-residue fragment containing the conserved CxCxxxxCxC motif is sufficient for Cu(I)-induced dimerization, challenging previous assumptions that a longer region is required.[22] Cu(I) binding leads to the formation of binuclear (Cu_2L) and dimeric (Cu_4L_2) complexes, whereas Zn(II) favors simpler monomeric and dimeric species. Spectroscopic analyses confirmed that both metals induce distinct structural transitions, with Cu(I) promoting more complex conformational rearrangements. Our results indicate that the metal-binding behavior of CopY's C-terminal motif is strongly influenced by the number and arrangement of cysteine residues. The presence of a single CxC motif, as in *Streptococcus pneumoniae* CopY, favors Cu_2L_2 dimer formation, whereas proteins with two CxC motifs (e.g., *Enterococcus hirae* CopY) preferentially form Cu_4L_2 clusters. Zn(II) coordination stabilizes a distinct structural fold, independent of the *M*:*L* ratio, which may be critical for the regulatory function of CopY in metal homeostasis.

Overall, our study highlights the intricate interplay between Cu(I)/Zn(II) ions and the C-terminal region of CopY, providing valuable insights into the metalation process and dimerization mechanisms in bacterial metalloregulation. These findings may contribute to a better understanding of how copper and zinc ions influence protein structure and function in metal homeostasis and antimicrobial resistance. Future work should aim to link these structural findings to functional consequences, such as DNA binding or protein−protein interactions, to fully elucidate the role of metal-induced conformational changes in CopY-mediated transcriptional control.

ASSOCIATED CONTENT

Supporting Information

The Supporting Information is available free of charge at https://pubs.acs.org/doi/10.1021/acs.inorgchem.5c03226.

The m/z values for both metal complexes at an *M*:*L* ratio of 0.9:1 (Table S1); Figures S1−S2−S3−S4-S5, Table S1; the 2D NOESY spectra displayed no inter-residue NOE correlations, indicating the absence of stable long-range contacts (Figure S1); the NMR spectrum following Zn(II) addition revealed several key effects (Figure S2); zinc coordination leaves the NMR line widths of the peptide signals unchanged and wellresolved, thereby indicating the formation of monomeric Zn(II) complexes (Figure S3); Fingerprint regions of 1H−1H NOESY of Ac-ECNCIPGQ-CECKKQ in the absence and in presence of 0.9 Zn(II) equivalents (Figure S4); the addition of copper led to a greater dispersion of the NH signals in the NMR spectrum (Figure S5); (PDF)

AUTHOR INFORMATION

Corresponding Author

Aleksandra Hecel − *Faculty of Chemistry, University of Wroclaw, Wroclaw 50383, Poland;* orcid.org/0000-0002-4314-9599; Email: aleksandra.hecel2@uwr.edu.pl

Authors

Arian Kola − *Department of Biotechnology, Chemistry and Pharmacy, University of Siena, Siena 53100, Italy; Department of Life Science, University of Siena, Siena 53100, Italy*

Alicia Dominguez-Martin − *Department of Inorganic Chemistry, Faculty of Pharmacy, University of Granada, Granada 18071, Spain;* orcid.org/0000-0001-8669-6712

Daniela Valensin − *Department of Biotechnology, Chemistry and Pharmacy, University of Siena, Siena 53100, Italy; Consorzio Interuniversitario Risonanze Magnetiche di Metalloproteine (CIRMMP), Sesto Fiorentino 50019, Italy*

Complete contact information is available at: https://pubs.acs.org/10.1021/acs.inorgchem.5c03226

Notes

The authors declare no competing financial interest.

ACKNOWLEDGMENTS

This work was supported by the National Science Centre, Poland (grant no. UMO-2023/51/D/ST5/01798), and by the Internal Grant of the Excellence Initiative − Research University (IDUB), University of Wroclaw (grant no. BPIDUB.13.2024). We gratefully acknowledge the support for academic staff mobility provided under the IDUB programme. A.D.M. acknowledges the Research Thematic Network RED2022-134091-T, financed by MCIN/AEI, and the Research Group FQM-283, Junta de Andalucía.

REFERENCES

(1) Capdevila, D.A.; Edmonds, K.A.; Giedroc, D.P. Metallochaperones and metalloregulation in bacteria. *Essays Biochem* **2017**, *61*, 177−200.

(2) Hossain, S.; Morey, J.; Neville, S.; Ganio, K.; Radin, J.; Norambuena, J.; Boyd, J.; McDevitt, C.; Kehl-Fie, T. Host subversion of bacterial metallophore usage drives copper intoxication. *Mbio* **2023**, *14* (5), No. e01350-23.

(3) Menezes, L.; Sampaio, R.; Meurer, L.; Szpoganicz, B.; Cervo, R.; Cargnelutti, R.; Wang, L.; Yang, J.; Prabhakar, R.; Fernandes, C.; et al. A Multipurpose Metallophore and Its Copper Complexes with Diverse Catalytic Antioxidant Properties to Deal with Metal and Oxidative Stress Disorders: A Combined Experimental, Theoretical, and In Vitro Study. *Inorg. Chem.* **2024**, *63* (32), 14827−14850.

(4) Novoa-Aponte, L.; Argüello, J. Unique underlying principles shaping copper homeostasis networks. *J. Biol. Inorg. Chem.* **2022**, *27* (6), 509−528.

(5) Portmann, R.; Magnani, D.; Stoyanov, J.; Schmechel, A.; Multhaup, G.; Solioz, M. Interaction kinetics of the copper-responsive CopY repressor with the cop promoter of Enterococcus hirae. *J. Biol. Inorg. Chem.* **2004**, *9* (4), 396−402.

(6) Cobine, P.; Jones, C.; Dameron, C. Role for zinc(II) in the copper(I) regulated protein CopY. *J. Inorg. Biochem.* **2002**, *88* (2), 192−196.
(7) Solioz, M.; Stoyanov, J. Copper homeostasis in Enterococcus hirae. *FEMS Microbiol. Rev.* **2003**, *27* (2−3), 183−195.
(8) Cobine, P.; George, G.; Jones, C.; Wickramasinghe, W.; Solioz, M.; Dameron, C. Copper transfer from the Cu(I) chaperone, CopZ, to the repressor, Zn(II)CopY: Metal coordination environments and protein interactions. *Biochemistry* **2002**, *41* (18), 5822−5829.
(9) Cobine, P.; Wickramasinghe, W.; Harrison, M.; Weber, T.; Solioz, M.; Dameron, C. The Enterococcus hirae copper chaperone CopZ delivers copper(I) to the CopY repressor. *FEBS Lett.* **1999**, *445* (1), 27−30.
(10) Neubert, M.J.; Dahlmann, E.A.; Ambrose, A.; Johnson, M.D.L. Copper Chaperone CupA and Zinc Control CopY Regulation of the Pneumococcal cop Operon. *MSphere* **2017**, *2* (5), 10−1128.
(11) Hendrixson, W. Further work on potassium hydrogen phthalate as a standard in volumetric analysis. *J. Am. Chem. Soc.* **1920**, *42*, 724−727.
(12) Buck, R.; Rondinini, S.; Covington, A.; Baucke, F.; Brett, C.; Camoes, M.; Milton, M.; Mussini, T.; Naumann, R.; Pratt, K.; et al. Measurement of pH. Definition, standards, and procedures. *Pure Appl. Chem.* **2002**, *74* (11), 2169−2200.
(13) Plonka, D.; Kotuniak, R.; Dabrowska, K.; Bal, W. Electrospray-Induced Mass Spectrometry Is Not Suitable for Determination of Peptidic Cu(II) Complexes. *J. Am. Soc. Mass Spectrom.* **2021**, *32* (12), 2766−2776.
(14) Wu, Z.; Fernandez-Lima, F.; Perez, L.; Russell, D. A New Copper Containing MALDI Matrix That Yields High Abundances of [Peptide + Cu]+ Ions. *J. Am. Soc. Mass Spectrom.* **2009**, *20* (7), 1263−1271.
(15) Prudent, M.; Girault, H. On-line electrogeneration of copper-peptide complexes in microspray mass spectrometry. *J. Am. Soc. Mass Spectrom.* **2008**, *19* (4), 560−568.
(16) Zhang, J.; Frankevich, V.; Knochenmuss, R.; Friess, S.; Zenobi, R. Reduction of Cu(II) in matrix-assisted laser desorption/ionization mass spectrometry. *J. Am. Soc. Mass Spectrom.* **2003**, *14* (1), 42−50.
(17) Iavorschi, M.; Lupaescu, A.; Darie-Ion, L.; Indeykina, M.; Hitruc, G.; Petre, B. Cu and Zn Interactions with Peptides Revealed by High-Resolution Mass Spectrometry. *Pharmaceuticals* **2022**, *15* (9), 1096.
(18) Gans, P.; O'Sullivan, B. GLEE, a new computer program for glass electrode calibration. *Talanta* **2000**, *51* (1), 33−37.
(19) Gans, P.; Sabatini, A.; Vacca, A. Investigation of equilibria in solution. Determination of equilibrium constants with the HYPERQUAD suite of programs. *Talanta* **1996**, *43* (10), 1739−1753.
(20) Alderighi, L.; Gans, P.; Ienco, A.; Peters, D.; Sabatini, A.; Vacca, A. Hyperquad simulation and speciation (HySS):A utility program for the investigation of equilibria involving soluble and partially soluble species. *Coord. Chem. Rev.* **1999**, *184*, 311−318.
(21) Hwang, T. L.; Shaka, A. J. WATER SUPPRESSION THAT WORKS - EXCITATION SCULPTING USING ARBITRARY WAVE-FORMS AND PULSED-FIELD GRADIENTS. *J. Magn. Reson., Ser. A* **1995**, *112* (2), 275−279.
(22) Pazehoski, K.; Cobine, P.; Winzor, D.; Dameron, C. Evidence for involvement of the C-terminal domain in the dimerization of the CopY repressor protein from Enterococcus hirae. *Biochem. Biophys. Res. Commun.* **2011**, *406* (2), 183−187.
(23) Miller, A.; Matera-Witkiewicz, A.; Mikolajczyk, A.; Watly, J.; Wilcox, D.; Witkowska, D.; Rowinska-Zyrek, M. Zn-Enhanced Asp-Rich Antimicrobial Peptides: N-Terminal Coordination by Zn(II) and Cu(II), Which Distinguishes Cu(II) Binding to Different Peptides. *IJMS* **2021**, *22* (13), 6971.
(24) Krzywoszynska, K.; Swiatek-Kozlowska, J.; Potocki, S.; Ostrowska, M.; Kozlowski, H. Triplet of cysteines − Coordinational riddle? *J. Inorg. Biochem.* **2020**, *204*, 110957.
(25) Witkowska, D.; Bielinska, S.; Kamysz, W.; Kozlowski, H. Cu2+ and Ni2+ interactions with N-terminal fragments of Hpn and Hpn-like proteins from Helicobacter pylori Unusual impact of poly-Gln sequence on the complex stability. *J. Inorg. Biochem.* **2011**, *105* (2), 208−214.
(26) Potocki, S.; Rowinska-Zyrek, M.; Valensin, D.; Krzywoszynska, K.; Witkowska, D.; Luczkowski, M.; Kozlowski, H. Metal Binding Ability of Cysteine-Rich Peptide Domain of ZIP13 Zn2+ Ions Transporter. *Inorg. Chem.* **2011**, *50* (13), 6135−6145.
(27) Rowinska-Zyrek, M.; Valensin, D.; Szyrwiel, L.; Grzonka, Z.; Kozlowski, H. Specific interactions of Bi(III) with the Cys-Xaa-Cys unit of a peptide sequence. *Dalton Trans.* **2009**, *42*, 9131−9140.
(28) Perinelli, M.; Tegoni, M.; Freisinger, E. Different Behavior of the Histidine Residue toward Cadmium and Zinc in a Cadmium-Specific Metallothionein from an Aquatic Fungus. *Inorg. Chem.* **2020**, *59* (23), 16988−16997.
(29) Roos, G.; Foloppe, N.; Messens, J. Understanding the pKa of Redox Cysteines: The Key Role of Hydrogen Bonding. *Antioxid. Redox Signal* **2013**, *18* (1), 94−127.
(30) Harris, T.; Turner, G. tructural basis of perturbed pKa values of catalytic groups in enzyme active sites. *IUBMB Life* **2002**, *53* (2), 85−98.
(31) Watly, J.; Hecel, A.; Wieczorek, R.; Swiatek-Korlowska, J.; Kozlowski, H.; Rowinska-Zyrek, M. Uncapping the N-terminus of a ubiquitous His-tag peptide enhances its Cu2+ binding affinity. *Dalton Trans.* **2019**, *48* (36), 13567−13579.
(32) Hecel, A.; Freisinger, E. Uncovering the copper(I) binding abilities of a unique fungal metallothionein: Characterization of Yarrowia lipolytica MT and its Y54C mutant. **2025**.
(33) Sigel, H.; Martin, R. B. Coordinating properties of the amide bond. Stability and structure of metal ion complexes of peptides and related ligands. *Chem. Rev.* **1982**, *82* (4), 385−426.
(34) Jakab, N.; Jancsó, A.; Gajda, T.; Gyurcsik, B.; Rockenbauer, A. Copper(II), nickel(II) and zinc(II) complexes of *N*-acetyl-His-Pro-His-His-NH_2: Equilibria, solution structure and enzyme mimicking. *J. Inorg. Biochem.* **2008**, *102* (7), 1438−1448.
(35) Kaminska, J.; Hecel, A.; Slowik, J.; Rombel-Bryzek, A.; Rowinska-Zyrek, M.; Witkowska, D. Characterization of four peptides from milk fermented with kombucha cultures and their metal complexes—in search of new biotherapeutics. *Front. Mol. Biosci.* **2024**, *11*, 1366588.
(36) Leveraro, S.; Dzyhovskyi, V.; Garstka, K.; Szebesczyk, A.; Zobi, F.; Bellotti, D.; Stokowa-Soltys, K.; Remelli, M.; Rowinska-Zyrek, M. Metal-Induced Amide Deprotonation and Binding Typical for Cu(II), Not Possible for Zn(II) and Fe(II). *Inorg. Chem.* **2025**, *64* (13), 6751−6760.
(37) Isik, M.; Rustenburg, A.; Rizzi, A.; Gunner, M.; Mobley, D.; Chodera, J. Overview of the SAMPL6 pKa challenge: Evaluating small molecule microscopic and macroscopic pKa predictions. *J. Comput.-Aided Mol. Des.* **2021**, *35* (2), 131−166.
(38) Middendorf, T.; Aldrich, R. The structure of binding curves and practical identifiability of equilibrium ligand-binding parameters. *J. Gen. Physiol.* **2017**, *149* (1), 121−147.
(39) Ribeiro, A.; Schmidt, T. Determination of acid dissociation constants (pKa) of. cephalosporin antibiotics: Computational and experimental approaches. *Chemosphere* **2017**, *169*, 524−533.
(40) Indelicato, S.; Bongiorno, D.; Ceraulo, L. Recent Approaches for Chemical Speciation and Analysis by Electrospray Ionization (ESI) Mass Spectrometry. *Front. Chem.* **2021**, *8*, 625945.
(41) van Dongen, W.; Heck, A. Binding of selected carbohydrates to apo-concanavalin A studied by electrospray ionization mass spectrometry. *The Analyst* **2000**, *125* (4), 583−589.
(42) Sun, J.; Kitova, E.; Klassen, J. Method for stabilizing protein-ligand complexes in nanoelectrospray ionization mass spectrometry. *Anal. Chem.* **2007**, *79* (2), 416−425.
(43) Clark, S.; Konermann, L. Determination of ligand-protein dissociation constants by electrospray mass spectrometry-based diffusion measurements. *Anal. Chem.* **2004**, *76* (23), 7077−7083.
(44) Robinson, C.; Chung, E.; Kragelund, B.; Knudsen, J.; Aplin, R.; Poulsen, F.; Dobson, C. Probing the nature of noncovalent interactions by mass spectrometry. A study of protein-CoA ligand binding and assembly. *J. Am. Chem. Soc.* **1996**, *118* (36), 8646−8653.

https://doi.org/10.1021/acs.inorgchem.5c03226
Inorg. Chem. 2025, 64, 22615−22630

(45) Krezel, A.; Maret, W. Dual nanomolar and picomolar Zn(II) binding properties of metallothionein. *J. Am. Chem. Soc.* **2007**, *129* (35), 10911−10921.
(46) Pomorski, A.; Drozd, A.; Kocyla, A.; Krezel, A. From methodological limitations to the function of metallothioneins-a guide to approaches for determining weak, moderate, and tight affinity zinc sites. *Metallomics* **2023**, *15* (5), mfad027.
(47) Chan, K.; Bakman, I.; Marts, A.; Batir, Y.; Dowd, T.; Tierney, D.; Gibney, B. Characterization of the Zn(II) Binding Properties of the Human Wilms' Tumor Suppressor Protein C-terminal Zinc Finger Peptide. *Inorg. Chem.* **2014**, *53* (12), 6309−6320.
(48) Brose, J.; La Fontaine, S.; Wedd, A.; Xiao, Z. Redox sulfur chemistry of the copper chaperone Atox1 is regulated by the enzyme glutaredoxin 1, the reduction potential of the glutathione couple GSSG/2GSH and the availability of Cu(I). *Metallomics* **2014**, *6* (4), 793−808.
(49) Niemiec, M.; Weise, C.; Wittung-Stafshede, P. In Vitro Thermodynamic Dissection of Human Copper Transfer from Chaperone to Target Protein. *PLoS One* **2012**, *7* (5), No. e36102. Xiao, Z.; Brose, J.; Schimo, S.; Ackland, S.; La Fontaine, S.; Wedd, A. Unification of the Copper(I) Binding Affinities of the Metallo-chaperones Atx1, Atox1, and Related Proteins DETECTION PROBES AND AFFINITY STANDARDS. *J. Biol. Chem.* **2011**, *286* (13), 11047−11055.
(50) Pomorski, A.; Otlewski, J.; Krezel, A. The High ZnII Affinity of the Tetracysteine Tag Affects Its Fluorescent Labeling with Biarsenicals. *ChemBiochem* **2010**, *11* (9), 1214−1218.
(51) Luczkowski, M.; Leszczynska, W.; Watly, J.; Clemens, S.; Krezel, A. Phytochelatins Bind Zn(II) with Micro- to Picomolar Affinities without the Formation of Binuclear Complexes, Exhibiting Zinc Buffering and Muffling Rather than Storing Functions. *Inorg. Chem.* **2024**, *63* (24), 10915−10931.
(52) Szunyogh, D.; Gyurcsik, B.; Larsen, F.; Stachura, M.; Thulstrup, P.; Hemmingsen, L.; Jancsó, A. ZnII and HgII binding to a designed peptide that accommodates different coordination geometries. *Dalton Trans.* **2015**, *44* (28), 12576−12588.
(53) Pountney, D.; Schauwecker, I.; Zarn, J.; Vasak, M. FORMATION OF MAMMALIAN CU-8-METALLOTHIONEIN IN-VITRO - EVIDENCE FOR THE EXISTENCE OF 2 CU(I)(4)-THIOLATE CLUSTERS. *Biochemistry* **1994**, *33* (32), 9699−9705.
(54) Tarasava, K.; Loebus, J.; Freisinger, E. Localization and Spectroscopic Analysis of the Cu(I) Binding Site in Wheat Metallothionein Ec-1. *Int. J. Mol. Sci.* **2016**, *17* (3), 371.
(55) Glauninger, H.; Zhang, Y.; Higgins, K.; Jacobs, A.; Martin, J.; Fu, Y.; Coyne, H.; Bruce, K.; Maroney, M.; Clemmer, D. E.; et al. Metal-dependent allosteric activation and inhibition on the same molecular scaffold: The copper sensor CopY from Streptococcus pneumoniae. *Chem. Sci.* **2018**, *9* (1), 105−118.
(56) Vasak, M.; Kagi, J.; Hill, H. ZINC(II), CADMIUM(II), AND MERCURY(II) THIOLATE TRANSITIONS IN METALLOTHIONEIN. *Biochemistry* **1981**, *20* (10), 2852−2856.

https://doi.org/10.1021/acs.inorgchem.5c03226
Inorg. Chem. 2025, 64, 22615−22630